
▮ LADDER: Language Driven Slice Discovery and Error Rectification

Shantanu Ghosh

Department of Electrical and Computer Engineering
Boston University
shawn24@bu.edu

Chenyu Wang

Department of Electrical and Computer Engineering
Boston University
chyuwang@bu.edu

Kayhan Batmanghelich

Department of Electrical and Computer Engineering
Boston University
batman@bu.edu

Abstract

Error slice discovery associates structured patterns with model errors. Existing methods discover error slices by clustering the error-prone samples with similar patterns or assigning discrete attributes to each sample for post-hoc analysis. While these methods aim for interpretability and easier mitigation through reweighting or rebalancing, they may not capture the full complexity of error patterns due to incomplete or missing attributes. Contrary to the existing approach, this paper utilizes the reasoning capabilities of the Large Language Model (LLM) to analyze complex error patterns and generate testable hypotheses. This paper proposes LADDER: Language Driven slice Discovery and Error Rectification. It first projects the model’s representation into a language-aligned feature space (*e.g.*, CLIP) to preserve semantics in the original model feature space. This ensures the accurate retrieval of sentences that highlight the model’s errors. Next, the LLM utilizes the sentences and generates hypotheses to discover error slices. Finally, we mitigate the error by fine-tuning the classification head by creating a group-balanced dataset using the hypotheses. Our entire method does not require any attribute annotation, either explicitly or through external tagging models. We validate our method with **five** image classification datasets. The code is available¹.

1 Introduction

Discovering systematic errors, or error slices, in predictive models is essential for understanding and mitigating their limitations. Traditional approaches to slice discovery often involve clustering misclassified samples based on attributes. Alternatively, they directly analyze these attributes to identify patterns associated with errors. While attribute-based methods are intuitive and facilitate straightforward mitigation strategies like rebalancing, they fundamentally lack the capacity for deeper reasoning about the underlying complexities of model errors. In contrast, our approach, termed

¹<https://github.com/batmanlab/Ladder>

LADDER, leverages the advanced reasoning capabilities of LLMs. By sidestepping the need for direct attribute association, LADDER initiates by retrieving sentences highlighting errors and then employing LLMs to formulate testable hypotheses from these sentences. In a fully automated fashion, LADDER effectively addresses both the discovery and rectification of error slices, utilizing language as a powerful tool for analysis and intervention.

Recent slice discovery algorithms utilize vision language representation (VLR) space to identify and subsequently interpret error slices. Examples include error-aware mixture models, *e.g.*, DOMINO [10], modality gap-based methods for CLIP encoders, *e.g.*, DrML [49], and data-driven approaches inducing strong spurious correlations in the source model, *e.g.*, FACTS [46]. Conversely, methods like PRIME [35] emphasize interpretability first by identifying tags for specific error slices. These methods encounter significant challenges due to: 1) their reliance on specific pretrained models that are not universally adaptable, *e.g.*, FACTS and Dr.ML; 2) the descriptions of error slices often suffering from semantic discrepancies, with attributes not consistently preserved within the VLR space, *e.g.*, DOMINO; 3) usage of expensive tagging models resulting in incomplete attribute tagging, *e.g.*, PRIME; 4) the lack of reasoning capabilities necessary to understand complex error patterns 5) the unavailability of suitable tagging models in fields *e.g.*, radiology, limiting their application in such specialized domains.

The literature on bias mitigation is extensive. For example, GroupDRO [37] emphasizes the critical role of regularization in achieving worst-case generalization across different groups. JTT [27] introduces a two-stage training process that enhances group robustness by re-weighting difficult examples without the need for explicit group labels in the training data. The causal method *e.g.*, [30] demonstrates the usage of auxiliary labels to strategically eliminate reliance on spurious correlations in predictive models. Recently, DFR [19] illustrates that re-training only the last layer of a neural network effectively mitigates the effects of spurious correlations. However, they all rely on group annotations in training/validation data, aiming to mitigate errors in a single slice. In contrast, LADDER utilizes language to discover and fix errors without group annotations across slices.

Contributions. Our contributions are two fold: 1) LADDER leverages language to discover error slices in any off-the-shelf pretrained model, overcoming the specific training dependencies in methods *e.g.*, FACTS and Dr.ML, or the expensive and incomplete tagging models used by PRIME. 2) LADDER effectively mitigates error across all slices without requiring the ground truth attributes. LADDER employs four key approaches to perform slice discovery and mitigation: 1) instead of projecting raw images directly into the VLR space (as done by DOMINO), LADDER projects the model’s representation. This ensures that LADDER focuses on those semantic attributes that the model considers relevant, providing a more accurate basis for identifying errors; 2) utilizing a corpus of image captions or radiology reports, it retrieves sentences indicative of errors that have a high similarity to the projected image representations; 3) it invokes LLM with the retrieved sentences to formulate testable hypotheses to reason for the model’s mistakes; 4) for each identified slice, LADDER constructs a group-balanced dataset, retrieving images that both conform to and deviate from the hypotheses, and then fine-tunes the model’s linear classification head to mitigate errors. LADDER outperforms **two** state-of-the-art (SOTA) slice discovery methods and achieves comparable results with **15** bias mitigation algorithms across **three** natural images and **two** real-world medical imaging datasets for both CNN and ViT architectures. To the best of our knowledge, LADDER is the first method that uses the reasoning capabilities of LLM to identify and fix model errors.

2 LADDER

Notation: Assume the classifier f predicts the labels \mathcal{Y} from the images \mathcal{X} , trained using ERM [41]. Assume $f = g \circ \Phi$, where Φ and g are the image representation and classification head, respectively. Additionally, $\{\Psi^I, \Psi^T\}$ denote the image and text encoders of the joint VLR space (*e.g.*, CLIP). For a set of images \mathcal{X}_Y of a class $Y \in \mathcal{Y}$, our method finds error slices where the model f underperforms and fixes it. LADDER employs a text corpus t_{val} from radiology reports or image captions. Note that we do not need paired image captions. Throughout the paper, $\langle \cdot, \cdot \rangle$ denotes the dot product to estimate the similarity between two representations. Fig. 1 shows the schematic of our method. Across our method, we do not assume the availability of sample-specific attributes, whether through annotation or human-generated prompts. LADDER utilizes the validation dataset (can be a small subset of training data, not used during training) to discover and mitigate errors.

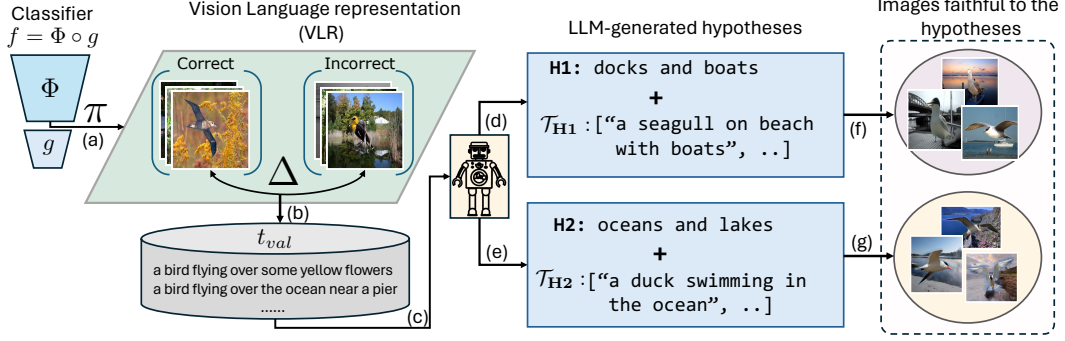


Figure 1: Schematic of slice discovery of LADDER. **(a)**: Projection (π) of model representation (Φ) to VLR space. **(b)**: Retrieval of $\text{top}K$ sentences based on the difference in image embeddings (Δ) within VLR space. **(c)**: LLM is invoked with $\text{top}K$ sentences. **(d-e)**: LLM generated hypotheses and sentences ($\{\mathcal{H}, \mathcal{T}\}$) to test the hypotheses. **(f-g)**: Finding the clusters faithful to the hypotheses.

Error slice: An error slice for a class Y includes subsets \mathcal{X}_Y where the model performs significantly worse than its overall performance on the entire class Y , formally defined as:

$$\mathcal{S}_Y = \{\mathcal{S}_{Y, \text{-attr}} \subseteq \mathcal{X}_Y | e(\mathcal{S}_{Y, \text{-attr}}) \gg e(\mathcal{X}_Y), \exists \text{attr}\},$$

where $e(\cdot)$ is the error rate on the specific data subset and $\mathcal{S}_{Y, \text{-attr}}$ denotes the subset of \mathcal{X}_Y without the attribute attr . Alternatively, f is biased on the attribute attr , resulting in better performance on the subpopulation with attr *e.g.*, error rate in pneumothorax patients without chest tubes is higher than that of overall pneumothorax patients.

2.1 Retrieving sentences highlighting model’s error

First, for a particular class, LADDER retrieves the sentences indicating the visual attributes present in the correctly classified samples but absent in the misclassified ones, causing the model’s error. Following [31], it learns a projection function $\pi : \Phi \rightarrow \Psi^I$ to align the representation of the classifier, Φ , with the image representation, Ψ^I of the joint VLR space. Then, for a class label Y , we estimate the difference in mean of the projected representations of the correct and misclassified samples as $\Delta^I = \mathbb{E}_{X, Y | f(X)=Y}[\pi(\Phi(X))] - \mathbb{E}_{X, Y | f(X) \neq Y}[\pi(\Phi(X))]$. Assuming the mean representations preserve semantics, this difference highlights the presence of pivotal attributes in correctly classified samples but is missing in misclassified samples. Denoting the text embedding of t_{val} as $\Psi^T(t_{val})$, we retrieve the $\text{top}K$ sentences as: $\text{top}K = \mathcal{R}(\langle \Delta^I, \Psi^T(t_{val}) \rangle, t_{val})$, where \mathcal{R} is a retrieval function retrieving $\text{top}K$ sentences from the text corpus having the highest similarity score with the mean difference of the projected image representations. We use these sentences to diagnose the model’s errors f by constructing hypotheses from LLM.

2.2 Hypothesis generation via LLM and discovering error slices

Hypothesis generation. To retrieve the set of hypotheses, LADDER invokes an LLM with the $\text{top}K$ sentences. Formally, $\{\mathcal{H}, \mathcal{T}\} = \text{LLM}(\text{top}K)$, where \mathcal{H} is a set of hypotheses with attributes on which f may be biased and \mathcal{T} is a set of sentences to be used to test each hypothesis. f underperforms on the subpopulation without the attributes in \mathcal{H} . Each hypothesis $H \in \mathcal{H}$ is paired with $\mathcal{T}_H \in \mathcal{T}$, a set of sentences that demonstrate the presence of the hypothesis-specific attribute in an image in various ways. Representations of images with the attribute specified in H , are highly similar to the mean text embedding of \mathcal{T}_H . Refer to Appendix B.1 for the prompts utilized by LLM to retrieve the sentences.

Discovering error slices. For each hypothesis $H \in \mathcal{H}$, we first compute the mean embedding of the set of sentences \mathcal{T}_H as $\Psi^T(\mathcal{T}_H) = \frac{1}{|\mathcal{T}_H|} \sum_{t \in \mathcal{T}_H} \Psi^T(t)$. Now for an image $X \in \mathcal{X}_Y$, we project to the VLR space as $\pi(\Phi(X))$ and compute the following similarity score,

$$s_H(X) = \langle \pi(\Phi(X)), \Psi^T(\mathcal{T}_H) \rangle \quad (1)$$

Finally, for a class label Y , we retrieve images with similarity scores below a threshold τ as $\mathcal{S}_{Y, \text{-}H} = \{X \in \mathcal{X}_Y | s_H(X) < \tau\}$. The hypothesis H fails in these images as they lack the attribute

specified in the H . The subset $\mathcal{S}_{Y,-H}$ may be a potential error slice, if the error $e(\mathcal{S}_{Y,-H})$ is greater than \mathcal{X}_Y . Formally, $\hat{\mathcal{S}}_Y$, the predicted slice for a class Y is:

$$\hat{\mathcal{S}}_Y = \{\mathcal{S}_{Y,-H} \subseteq \mathcal{X}_Y | e(\mathcal{S}_{Y,-H}) \gg e(\mathcal{X}_Y), \exists H \in \mathcal{H}\}, \quad (2)$$

2.3 Mitigating errors without annotation

Motivated by DFR [19], LADDER mitigates the error only by fine-tuning the model’s classification head. DFR [19] suggests that deep models already learn sufficiently informative representations to predict minority subpopulations correctly. Thus, fine-tuning only the classification head g mitigates errors on the specific error slice. To do so, DFR constructs group-balanced validation dataset \mathcal{D}_{bal} by ensuring equal representation of discrete ground truth attributes across positive and negative sets for each class (*e.g.*, pneumothorax patients with and without tubes, etc.). Unlike DFR, LADDER does not rely on the ground truth attributes. Instead, it utilizes a similarity score s_H (Eq. 1) for each hypothesis H to construct the hypotheses-balanced \mathcal{D}_{bal} . Specifically, LADDER selects images that align with H as well as those where H fails, thereby forming the respective positive and negative sets for fine-tuning g . To mitigate the error, we consider two scenarios where we want to fix the error on 1) a specific slice and 2) all the slices. For the 2nd case, we discuss two strategies for fixing the error. Note that in any of the following strategies, we don’t have access to the ground truth attributes in train/val datasets.

Scenario 1: Fixing the error of a specific slice. In this scenario, we want to fix the error in a particular subpopulation, *e.g.*, the absence of chest tubes in pneumothorax patients. However, LADDER does not require sample-specific attribute (tube annotation in this example) annotations for the train/val/test datasets. Firstly, from the hypothesis set \mathcal{H} , LADDER determines which hypothesis is closely related to the specific subpopulation where we aim to fix the error. Assuming `sub_pop_phrase` be the English phrase of denoting the subpopulation, we calculate the similarity score between the text embedding of `sub_pop_phrase` and all the hypotheses $H \in \mathcal{H}$ using the text encoder Ψ^T . Then, we chose the hypothesis with the highest similarity score. Formally:

$$H^* = \arg \max_{H \in \mathcal{H}} (\langle \Psi^T(\mathcal{T}_H), \Psi^T(\text{sub_pop_phrase}) \rangle) \quad (3)$$

Finally, we fine-tune g with \mathcal{D}_{bal} , balanced with H^* only. We call this DFR w/ slice info.

Scenario 2.1: Fixing the error on all slices using sequential fine-tuning. This strategy aims to fix errors on all the discovered slices. For each $H \in \mathcal{H}$, we create a balanced dataset \mathcal{D}_{bal} , and then fine-tune the classification head g . This fine-tuning process is executed sequentially, starting with the balanced dataset for the first hypothesis, fine-tuning the classifier, and proceeding to the next hypothesis, and so on. The process repeats till all hypotheses in \mathcal{H} are covered. We call this DFR w/ seq tune.

Scenario 2.2: Fixing the error on all slices using an ensemble approach. Although sequential tuning is effective, it risks the classifier forgetting representations learned from earlier hypotheses. In contrast, [24] uses a dynamic ensemble of classifiers each trained for specific data perturbations, enabling adaptive classifier selection based on distributional shifts. However, these classifiers specialize only in inputs resembling their training augmentations. LADDER creates \mathcal{D}_{bal} for each hypothesis H in \mathcal{H} and fine-tune a corresponding classifier head g_H . For a test image during inference, we select the classifier head g_{H^*} associated with the hypothesis that has the maximum similarity with the test image, where $H^* = \arg \max_{H \in \mathcal{H}} (s_H(X))$. We term this strategy DFR w/ ensemble.

3 Experiments

We conduct experiments to answer the following research questions: **RQ1.** How do different components of our slice discovery method contribute qualitatively? **RQ2.** How effective is our slice discovery method quantitatively compared to the baselines? **RQ3.** How effective is our mitigation algorithm compared to the baselines? **RQ4.** How do our mitigation algorithms effectively improve the performance of various slices? **Additional experiments.** We perform additional experiments to show 1) language can be used as an alternative to the ground truth attributes to analyze errors (Appendix B.9.1); 2) the statistical significance of the subsets identified by the LLM-generated hypotheses (Appendix B.9.2); and 3) the impact of using different variants of VLR space on NIH-CXR (Appendix B.9.3), respectively.

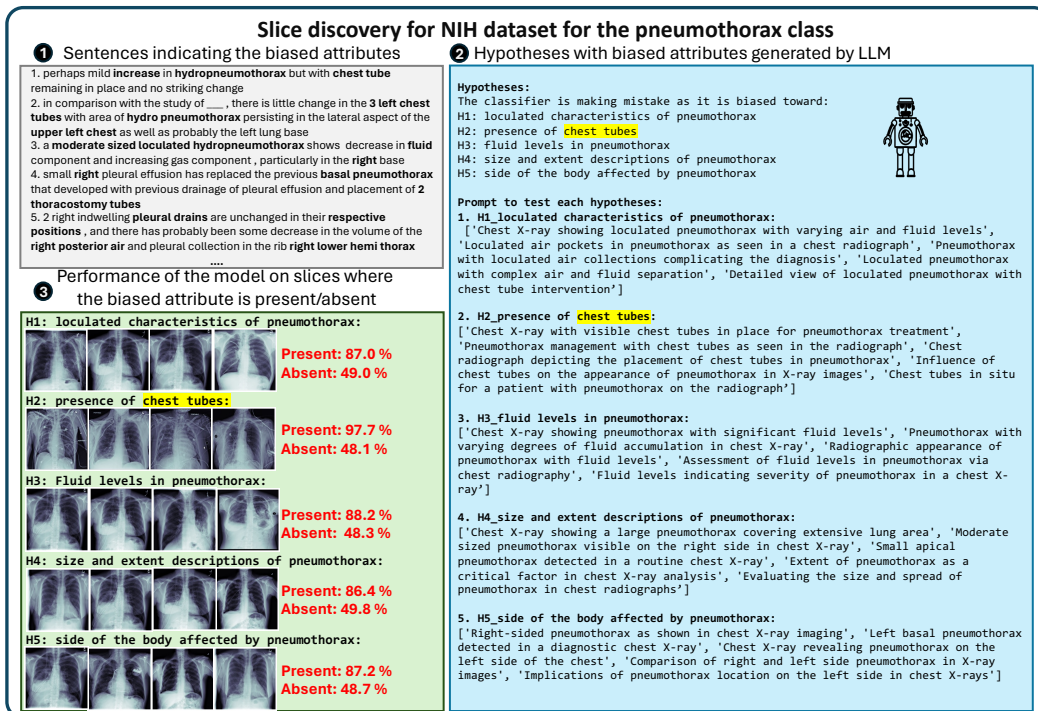
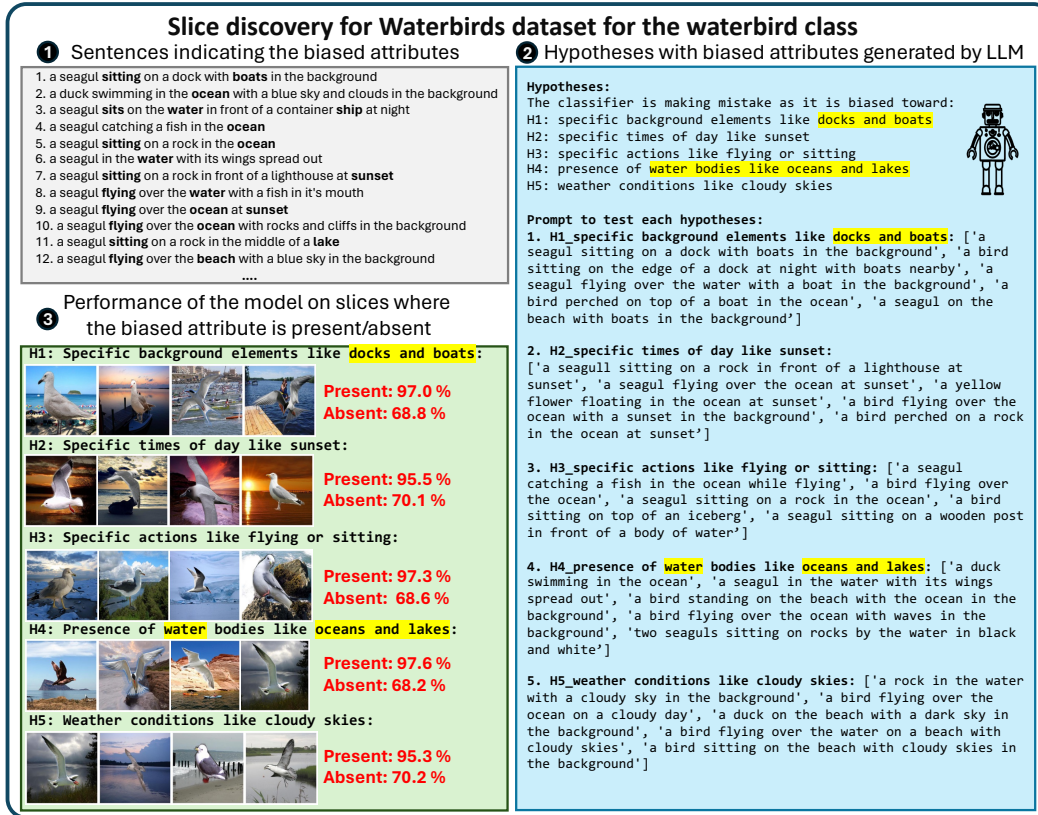


Figure 2: LADDER discovers slices for biased attributes in RN50-based classifiers. Both panels illustrate 1) the retrieval of sentences containing biased attributes (Sec. 2.1); 2) hypotheses generated by an LLM (Sec. 2.2); and 3) discovering error slices where the biased attribute does not present and *f* underperforms. We highlight the hypotheses indicative of the ground truth biased attribute (e.g., water for waterbirds or chest tube in pneumothorax patients for NIH-CXR) in **yellow**.

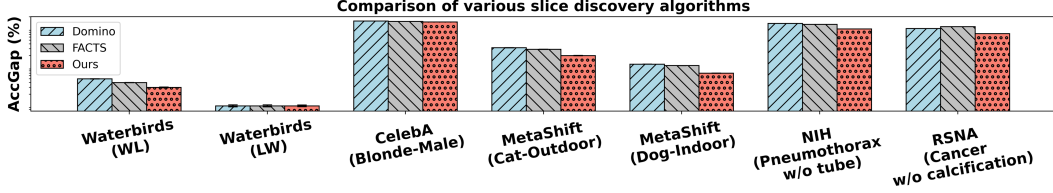


Figure 3: Comparisons of AccGap across various datasets for CNN-based slice discovery algorithms. Lower AccGap values indicate better performance in approximating true error slices, plotted on a logarithmic scale for clarity. WL and LW denote waterbirds on land and vice versa, respectively.

3.1 Datasets

We utilize 3 natural image classification datasets and 2 medical imaging datasets for the following classification tasks: 1) landbird vs waterbird using **Waterbirds** [42] where the background (most landbirds shown on land background and vice-versa) is spuriously correlated; 2) hair color (blond vs non blond) classification using **CelebA** [29] with the gender of the person serves as a spurious feature, as 94% of the images with the “blond” label, depict females, 3) cat vs dog classification using **MetaShift** where the background is the spurious correlation (most dogs are in outdoors vs most cat are indoors); 4) pneumothorax classification from chest-x-rays (CXR) using **NIH** dataset [43], with chest tube being the source of shortcut [8] (most pneumothorax patients having the chest tube); 5) breast cancer classification using the **RSNA-Mammo**² dataset with calcification being the shortcut (most cancer patients have calcifications). We discuss the datasets in detail in the Appendix B.2.

3.2 Baselines

Slice discovery. We compare LADDER with **Domino** [10] and **First Amplify Correlations and Then Slice (FACTS)** [46]. We discuss them in detail in Appendix B.3 **Error mitigation.** We compare our mitigation strategy with 15 baselines with different mitigation strategies: 1) *vanilla*: **ERM** [41]; 2) *subgroup robust methods*: **GroupDRO** [37], **CVaRDRO** [9], **LfF** [33], **JTT** [27], **LISA**, [45], **DFR** [14]; 3) *data augmentation*: **Mixup** [48]; 4) *domain-invariant representation learning*: **IRM** [2], **MMD** [23]; 4) *imbalanced learning*: **Focal** [26], **CBLoss** [6], **LDAM** [3], **CRT** [17], **ReWeightCRT** [17]. We discuss all of them in detail in Appendix B.4. We adopt the setting from [44] where ground truth attributes are available only in the validation data³.

3.3 Evaluation metrics

Slice discovery. As per [10, 46], we use Precision@10 to quantitatively evaluate the efficacy of the slice discovery methods on retrieving the ground truth (e.g., landbird on water) slices. We propose a new metric to compare the performance of different slice discovery algorithms by evaluating a discovered slice (e.g., waterbirds without boats) against a closely related ground truth slice (e.g., waterbirds not on water). Formally,

AccGap: This metric quantifies the absolute difference in accuracy between the ground truth error slice (w/o a specific attribute) and the predicted slice (the subset of data that doesn’t follow the top 3 closest matching hypothesis).

$$\text{AccGap} = \left| \frac{1}{|\mathcal{S}_{Y, \text{-attr}}|} \sum_{X \in \mathcal{S}_{Y, \text{-attr}}} \mathbf{1}\{f(X) = Y\} - \frac{1}{3} \sum_{i=1}^3 \left(\frac{1}{|\mathcal{S}_{Y, \text{-}H_i^*}|} \sum_{X \in \mathcal{S}_{Y, \text{-}H_i^*}} \mathbf{1}\{f(X) = Y\} \right) \right|, \quad (4)$$

where $\mathcal{S}_{Y, \text{-attr}}$ is the ground truth error slice with class Y and w/o the attribute attr ; $\mathcal{S}_{Y, \text{-}H_i^*}$ is the predicted error slice with class Y and not following the hypothesis H_i^* . We compute the top 3 hypotheses $\{H_i^*\}_{i=1}^3$, closest to the attribute attr using Eq. 3. For Domino and FACTS, we use the top5 captions per slice to discover the top3 error slices using Eq. 3 and finally compute **AccGap**.

²<https://www.kaggle.com/competitions/rsna-breast-cancer-detection>

³<https://github.com/YyzHarry/SubpopBench>

Table 1: Performance comparison of CNN-based error mitigation methods, measured over 3 seeds. We highlight the best results in bold and the second best in underlined.

Method	Waterbirds		CelebA		NIH		RSNA	
	Mean(%)	WGA(%)	Mean(%)	WGA(%)	Mean(%)	WGA(%)	Mean(%)	WGA(%)
Vanilla (ERM)	88.2 \pm 0.7	69.1 \pm 1.2	94.1 \pm 0.2	62.2 \pm 1.5	86.8 \pm 0.0	60.3 \pm 0.0	<u>85.3</u> \pm 0.0	69.8 \pm 0.0
Mixup	88.5 \pm 0.5	77.3 \pm 0.5	94.5 \pm 0.1	57.8 \pm 0.8	85.1 \pm 0.0	71.6 \pm 0.8	84.5 \pm 0.0	64.8 \pm 0.0
IRM	88.1 \pm 0.2	74.3 \pm 0.1	<u>94.5</u> \pm 0.5	63.3 \pm 2.5	83.2 \pm 0.0	63.4 \pm 0.0	83.3 \pm 0.0	68.4 \pm 0.0
MMD	92.5 \pm 0.1	83.5 \pm 1.1	92.5 \pm 0.6	22.7 \pm 2.5	84.6 \pm 0.0	65.4 \pm 0.0	84.2 \pm 0.0	69.1 \pm 0.0
Focal	89.3 \pm 0.2	71.6 \pm 0.8	94.9 \pm 0.3	59.3 \pm 2.0	85.5 \pm 0.0	70.9 \pm 0.7	83.6 \pm 0.0	65.5 \pm 0.0
CBLoss	91.3 \pm 0.7	86.1 \pm 0.3	91.2 \pm 0.7	89.3 \pm 0.5	85.5 \pm 0.0	71.4 \pm 0.0	83.2 \pm 0.0	65.1 \pm 0.0
LDAM	91.3 \pm 0.7	86.1 \pm 0.3	<u>94.5</u> \pm 0.2	58.3 \pm 2.5	84.3 \pm 0.0	69.4 \pm 0.2	81.6 \pm 0.0	63.5 \pm 0.0
CRT	90.5 \pm 0.0	79.7 \pm 0.3	92.5 \pm 0.1	87.3 \pm 0.3	82.7 \pm 0.0	68.5 \pm 0.0	82.7 \pm 0.0	68.8 \pm 0.0
ReWeightCRT	91.3 \pm 0.1	78.4 \pm 0.1	92.5 \pm 0.2	87.2 \pm 0.5	83.0 \pm 0.0	69.5 \pm 0.0	82.4 \pm 0.0	68.3 \pm 0.0
JTT	88.8 \pm 0.7	73.2 \pm 0.3	90.6 \pm 2.2	68.2 \pm 7.5	85.1 \pm 0.0	72.9 \pm 0.0	84.6 \pm 0.0	70.5 \pm 0.0
GroupDRO	88.8 \pm 1.7	76.2 \pm 1.3	91.4 \pm 0.6	<u>89.1</u> \pm 0.7	85.2 \pm 0.0	70.1 \pm 0.0	85.1 \pm 0.0	72.2 \pm 0.0
CVaRDRO	89.8 \pm 0.4	75.2 \pm 2.3	<u>94.5</u> \pm 0.1	63.1 \pm 1.5	85.7 \pm 0.1	72.1 \pm 0.0	85.4 \pm 0.0	72.1 \pm 0.0
LfF	87.0 \pm 0.3	75.2 \pm 0.7	81.1 \pm 5.6	53.0 \pm 4.4	75.9 \pm 0.0	60.0 \pm 0.0	79.8 \pm 0.0	62.4 \pm 0.0
LISA	92.8 \pm 0.3	88.7 \pm 0.6	92.6 \pm 0.1	86.2 \pm 1.1	85.2 \pm 0.0	73.6 \pm 0.0	85.1 \pm 0.0	72.4 \pm 0.0
DFR _{val}	<u>92.3</u> \pm 0.2	90.8 \pm 0.3	89.3 \pm 0.2	88.1 \pm 1.1	86.1 \pm 0.0	72.5 \pm 0.0	85.2 \pm 0.0	73.7 \pm 0.0
DFR w/ slice info (ours)	<u>92.3</u> \pm 0.8	<u>93.3</u> \pm 0.4	89.8 \pm 0.7	87.2 \pm 0.8	86.2 \pm 0.0	71.5 \pm 0.0	85.1 \pm 0.0	72.8 \pm 0.0
DFR w/ seq tune (ours)	91.4 \pm 0.6	<u>92.2</u> \pm 0.3	89.2 \pm 1.5	86.4 \pm 1.4	86.0 \pm 0.0	<u>75.2</u> \pm 0.0	86.1 \pm 0.0	76.4 \pm 0.0
DFR w/ ensemble (ours)	88.5 \pm 0.8	93.7 \pm 0.8	87.7 \pm 1.2	89.2 \pm 0.4	85.3 \pm 0.0	76.2 \pm 0.0	85.1 \pm 0.0	<u>75.7</u> \pm 0.0

Error mitigation. Following existing work on error mitigation, we report worst group accuracy (WGA) and mean accuracy for natural images across all algorithms. WGA refers to the accuracy of the worst-performing subgroup. For medical images, we report the mean AUROC. Specifically, for NIH-CXR and RSNA-Mammo, we define WGA as the performance on the subset of pneumothorax cases without chest tubes and cancer cases without calcification, respectively.

3.4 Experimental details

For natural images, we resize all the images to 224×224 and train imagenet pretrained CNN using Resnet-50 (RN50) [12] and vision transformer (ViT) models (as f) following in [44]. For NIH-CXR, we train an RN50 model with 224×224 images. For RSNA-Mammo, we resize the images to 1520×912 and train an EfficientNet (EN)-B5 model [40]. We utilize ViT-B/32 variant of CLIP [34], CXR-CLIP [47] (pretrained with MIMIC-CXR and CheXpert), and a vision language model trained with an in-house mammogram-report pair (refer to Appendix B.7.1) as **VLR space** ($\{\Psi^I, \Psi^T\}$) for natural images, NIH-CXR and RSNA-Mammo datasets respectively. For **the text corpus**, t_{val} , we utilize BLIP-captioner [21] to generate captions for the validation sets of the natural images. For NIH-CXR and RSNA-Mammo, we utilize the radiology reports from MIMIC-CXR [16] and a large corpus of in-house reports, respectively. We train **the projection function** π using [31]. For the **retrieval step** (topk in Sec.2.1), we retrieve 200 sentences for natural images and 100 sentences for medical images to generate hypotheses. We generate **hypotheses** using GPT-4V [1] as LLM. Finally, we use the same hyperparameters as the original model to fine-tune **the classification head** (h). Appendix B.7 illustrates additional experimental details and hyperparameters.

4 Results

Impact of different components on slice discovery (RQ1). Fig. 2 demonstrates the qualitative evaluation of LADDER in discovering error slices for classifying waterbirds (*top*) and pneumothorax (*bottom*) in the Waterbirds and NIH-CXR datasets for RN-50 models, respectively. Waterbirds are spuriously correlated with water backgrounds; correctly classified samples by the model f contain water-related attributes, while misclassified samples lack such backgrounds. Recall that the first step (Sec. 2.1) in LADDER retrieves the sentences with attributes present in correctly classified samples but absent in misclassified samples. In classifying waterbirds (Fig. 2 top panel, top-left), the retrieved sentences highlight attributes like boat, lake, and ocean, all capturing the ground truth water attribute in different forms. In the second step (Fig. 2 top panel, top-right), the LLM generates hypotheses and sentences to test the presence of these attributes in an image (as discussed in Sec. 2.2). The LLM correctly formulates the hypotheses based on the biased attributes and also generates the sentences to test each of them. In the third step (Fig. 2 top panel, bottom-left), LADDER validates

if the absence of these attributes leads the model f to underperform. For *e.g.*, subsets containing docks and boats (indicative of the water attribute) achieve an accuracy of 97%, whereas slices without these attributes (predicted error slice) achieve an accuracy of 68.8%. This aligns with prior findings that f fails to classify waterbirds not in water. We also visualize images with these attributes. Consistent with prior works [8], LADDER successfully captures chest tube as a source of spuriousness for NIH-CXR dataset (Fig. 2 bottom panel). The model f achieves an accuracy of 97.7% on pneumothorax patients with tube and 48.1% for patients without tube (predicted error slice). Appendix B.9.5 reports additional results across various datasets and architectures.

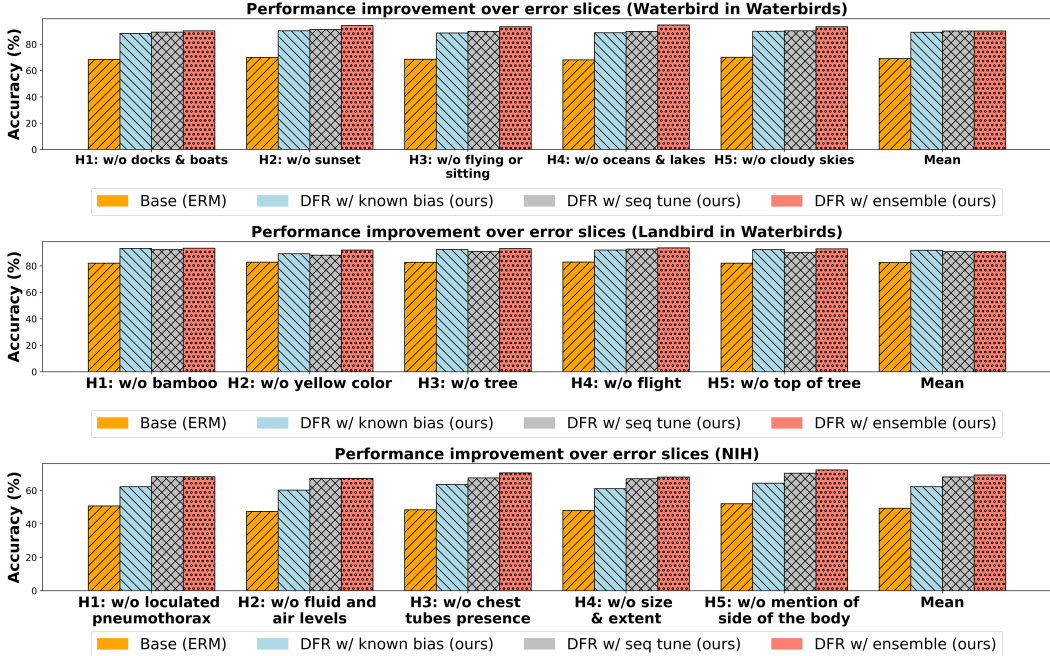


Figure 4: Accuracy improvements over error slices for our mitigation strategies compared to ERM.

Quantitative comparison with slice discovery algorithms (RQ2). Table 2 shows the Precision@10 for different slice discovery algorithms on CNN models. LADDER performs comparably to the baselines for natural images. For medical images, it outperforms the baselines, with improvements of 50% \uparrow for NIH-CXR and RSNA-Mammo. Figure 3 illustrates the AccGap for all slice discovery methods across CNN models. AccGap measures the accuracy gap between the ground truth and predicted error slices. For *e.g.*, in MetaShift, images of dogs are biased by the outdoor attribute. For the RN50 model, hypotheses generated by the LLM (Sec. 2.2) identify televisions, windows, and beds as the biased attributes most associated with outdoor (in Tab. 5). We compute the AccGap with images of the predicted error slice (*i.e.*, images of dogs lacking the predicted attributes) and the ground truth slice (*i.e.*, images without outdoor attributes). LADDER consistently exhibits the lowest AccGap, indicating that the model f underperforms similarly on the discovered error slices as on the ground truth slices. Appendix B.9.4 details the attributes identified by LADDER. FACTS and Domino use unsupervised clustering-based approaches by estimating the cross-modal embeddings of the images directly. In contrast, we first project the model’s representation Φ to VLR space, preserving the nuanced semantics of f . Additionally, the sentences identified in Sec. 2.1 help the LLM generate the hypotheses targeting specific attributes, causing the error slices. Finally, we explicitly compare the performance of f on subsets with or without the predicted attributes, leading to superior error slice discovery compared to the baselines. This result shows that the hypotheses generated by LLM correctly captures the ground truth attribute using sentences.

Comparison with various bias mitigation algorithms (RQ3) Table 1 compares our mitigation strategies with different baselines for CNN models (EN-B5 for RSNA Mammo & RN-50 for the rest). Our method consistently exhibit comparable performance against most of the baselines without access to the ground truth annotations for training and validation datasets. DFR w/ ensemble achieves WGA scores of 93.7%, an approximate increase of 2.7% over DFR_{val} in the Waterbirds dataset. For

the NIH dataset, both DFR w/ seq tune and DFR w/ ensemble outperform JTT by 2.3% and 3.3% respectively, and also surpass DFR_{val}'s score of 72.5%. Moreover, in the RSNA dataset, DFR w/ seq tune achieves a WGA score of 76.4% (a 3.6% \uparrow over DFR_{val}). DFR w/ ensemble follows closely with a 2% improvement, emphasizing the efficacy of our targeted mitigation strategies. This improvement is highly important in medical imaging, where accurately addressing minority subpopulations is critical. These results suggest that the slices identified by our hypotheses accurately represent the underlying ground truth biases. Additionally, our approach of using hypothesis-driven error slice identification and targeted mitigation strategies effectively enhances model performance, especially within minority subpopulations. The superior WGA scores achieved by our methods highlight their robustness and broad applicability across both vision and medical datasets. Appendix B.9.6 reports the same for ViT-based models for Waterbirds and CelebA.

Improving the performance over various slices (RQ4).

Figure 4 illustrates how different variants of our DFR (w/o attributes) model improve the performance of various slices compared to the initial model (trained with ERM) for Waterbirds and NIH-CXR datasets for RN50 architecture. For *e.g.*, , DFR w/ ensemble strategy improves the performance by >20% for all the slices in the NIH-CXR dataset. Among the different variants, DFR w/ ensemble consistently outperforms the other variants. Recall DFR w/ ensemble trains hypothesis-specific classifiers.

During inference, it evaluates the outputs from the classifiers and selects the prediction from the classifier's best match based on the hypothesis similarity score. This strategy reduces the risk of overfitting to specific attributes that might dominate in a single classifier scenario. It allows each classifier to become highly effective at recognizing and correctly classifying images from its respective slice.

Table 2: Precision@10 across datasets.

Dataset	Domino	FACTS	Ours
Waterbirds (Waterbird-Land)	0.8	1.0	1.0
Waterbirds (Landbird-Water)	1.0	1.0	1.0
CelebA (Blonde-Male)	0.9	0.9	0.9
MetaShift (Cat-Outdoor)	0.5	0.6	0.5
MetaShift (Dog-Indoor)	0.8	0.8	0.8
NIH (Pneumothorax-w/o tube)	0.6	0.6	0.9
RSNA (Cancer-w/o calcification)	0.4	0.4	0.6

5 Related Work

Slice discovery. Early slice discovery methods focus on tabular data employing predicates to define slices (*e.g.*, nationality = Indian) [4, 5, 36]. These methods struggle with unstructured data (*e.g.*, image or audio) due to the lack of coherent structure. Early works on unstructured data include [7, 39, 18, 38]. They typically project data into a representation space and identify error slices using clustering or dimensionality reduction techniques. They are primarily assessed through limited slice configurations or qualitative analysis. Recent works include the usage of VLR space [10, 15, 46, 49] for slice discovery. Specifically, DOMINO [10] projects images into the VLR space, identifies slices with a mixture model, and captions the slices. FACTS [46] begins by training a model to induce spurious correlations, then employs VLR to identify slices. Both approaches compromise the preservation of visual semantics within the VLR space, leading to semantic discrepancies in the descriptions of the slices. DrML leverages modality gap geometry and user-defined prompts to probe a CLIP encoder-based classifier, thereby introducing potential biases from human subjectivity. Further, FACTS and DrML are tailored to specific models or training regimes and cannot be readily applied to any pretrained model, limiting their applicability. Recently, PRIME [35] proposes an interpretability-first approach using tagging models to discover error-causing attributes. However, it faces limitations due to the potential incompleteness of tags and is constrained in domains where such tagging models are unavailable. **Error mitigation.** Error mitigation aims to improve the subgroup's performance where the model performs worst. GroupDRO [37] prioritizes groups with high error rates to improve upon ERM. CVaRDRO [9] adjusts weights dynamically for samples with high losses, enhancing distributional robustness. LfF trains a biased model along a de-biased counterpart, adjusting the loss gradients. JTT [27] identifies minority groups using an initial ERM model, then re-weights these in a training phase to address imbalances. DFR [14] re-trains only the final layer of a model using a balanced validation set to correct biases. All these methods use group annotation in training or validation data and aim to mitigate errors within a specific group. LADDER addresses all the limitations of the existing error discovery and mitigation approaches. It uses language to effectively discover error slices from any pretrained model without relying on external tags. Next, it mitigates errors across slices without any group annotation.

6 Conclusion and limitation

This paper presents LADDER, an automated framework for error slice discovery and mitigation that utilizes natural language and LLM reasoning without relying on external tags. It generates hypotheses to detect model errors and mitigates these through group-balanced datasets tailored to each identified slice. Extensive experiments illustrate the LADDER’s efficacy than the baselines. However, its performance depends on the quality of the available captions. Also, LADDER relies heavily on the quality of the vision language model. Future work will focus on refining the discovery process iteratively based on slice complexity and usage of language inversion to remove the requirement of the text corpus. Also, we will explore compositionality in hypothesis generation and evaluation.

References

- [1] Josh Achiam, Steven Adler, Sandhini Agarwal, Lama Ahmad, Ilge Akkaya, Florencia Leoni Aleman, Diogo Almeida, Janko Altenschmidt, Sam Altman, Shyamal Anadkat, et al. Gpt-4 technical report. *arXiv preprint arXiv:2303.08774*, 2023.
- [2] Martin Arjovsky et al. Invariant risk minimization. 2019.
- [3] Kaihua Cao et al. Learning imbalanced datasets with label-distribution-aware margin loss. 2019.
- [4] Mayee Chen, Karan Goel, Nimit S Sohoni, Fait Poms, Kayvon Fatahalian, and Christopher Ré. Mandoline: Model evaluation under distribution shift. In *International conference on machine learning*, pages 1617–1629. PMLR, 2021.
- [5] Yeounoh Chung, Tim Kraska, Neoklis Polyzotis, Ki Hyun Tae, and Steven Euijong Whang. Slice finder: Automated data slicing for model validation. In *2019 IEEE 35th International Conference on Data Engineering (ICDE)*, pages 1550–1553. IEEE, 2019.
- [6] Yin Cui et al. Class-balanced loss based on effective number of samples. 2019.
- [7] Greg d’Eon, Jason d’Eon, James R Wright, and Kevin Leyton-Brown. The spotlight: A general method for discovering systematic errors in deep learning models. In *Proceedings of the 2022 ACM Conference on Fairness, Accountability, and Transparency*, pages 1962–1981, 2022.
- [8] Frédéric Docquier and Hillel Rapoport. Globalization, brain drain, and development. *Journal of economic literature*, 50(3):681–730, 2012.
- [9] John Duchi and Hongseok Namkoong. Learning models with uniform performance via the convex fairness criterion. 2018.
- [10] Sabri Eyuboglu, Maya Varma, Khaled Saab, Jean-Benoit Delbrouck, Christopher Lee-Messer, Jared Dunnmon, James Zou, and Christopher Ré. Domino: Discovering systematic errors with cross-modal embeddings. *arXiv preprint arXiv:2203.14960*, 2022.
- [11] Arthur Gretton et al. A kernel two-sample test. 2012.
- [12] Kaiming He, Xiangyu Zhang, Shaoqing Ren, and Jian Sun. Deep residual learning for image recognition. In *Proceedings of the IEEE conference on computer vision and pattern recognition*, pages 770–778, 2016.
- [13] Issam Idrissi et al. Certified data removal from machine learning models. 2022.
- [14] Issam Imazilov et al. Certified data removal from machine learning models. 2022.
- [15] Saachi Jain, Hannah Lawrence, Ankur Moitra, and Aleksander Madry. Distilling model failures as directions in latent space. *arXiv preprint arXiv:2206.14754*, 2022.
- [16] Alistair EW Johnson, Tom J Pollard, Seth J Berkowitz, Nathaniel R Greenbaum, Matthew P Lungren, Chih-ying Deng, Roger G Mark, and Steven Horng. Mimic-cxr, a de-identified publicly available database of chest radiographs with free-text reports. *Scientific data*, 6(1):317, 2019.

- [17] Bingyi Kang et al. Decoupling representation and classifier for long-tailed recognition. 2020.
- [18] Michael P Kim, Amirata Ghorbani, and James Zou. Multiaccuracy: Black-box post-processing for fairness in classification. In *Proceedings of the 2019 AAAI/ACM Conference on AI, Ethics, and Society*, pages 247–254, 2019.
- [19] Polina Kirichenko, Pavel Izmailov, and Andrew Gordon Wilson. Last layer re-training is sufficient for robustness to spurious correlations. *arXiv preprint arXiv:2204.02937*, 2022.
- [20] Ranjay Krishna et al. Visual genome: Connecting language and vision using crowdsourced dense image annotations. 2016.
- [21] Junnan Li, Dongxu Li, Caiming Xiong, and Steven Hoi. Blip: Bootstrapping language-image pre-training for unified vision-language understanding and generation. In *International conference on machine learning*, pages 12888–12900. PMLR, 2022.
- [22] Yangguang Li, Feng Liang, Lichen Zhao, Yufeng Cui, Wanli Ouyang, Jing Shao, Fengwei Yu, and Junjie Yan. Supervision exists everywhere: A data efficient contrastive language-image pre-training paradigm. *arXiv preprint arXiv:2110.05208*, 2021.
- [23] Yuchao Li et al. Maximum mean discrepancy for domain adaptation. 2018.
- [24] Zhiheng Li, Ivan Evtimov, Albert Gordo, Caner Hazirbas, Tal Hassner, Cristian Canton Ferrer, Chenliang Xu, and Mark Ibrahim. A whac-a-mole dilemma: Shortcuts come in multiples where mitigating one amplifies others. In *Proceedings of the IEEE/CVF Conference on Computer Vision and Pattern Recognition*, pages 20071–20082, 2023.
- [25] Paul Pu Liang and James Zou. Metashift: A dataset for evaluating classifier robustness against natural distribution shifts. 2022.
- [26] Tsung-Yi Lin et al. Focal loss for dense object detection. 2017.
- [27] Ange Liu et al. Just train twice: Improving group robustness without training group information. 2021.
- [28] Ziwei Liu, Ping Luo, Xiaogang Wang, and Xiaoou Tang. Deep learning face attributes in the wild. *Proceedings of the IEEE International Conference on Computer Vision (ICCV)*, 2015.
- [29] Ziwei Liu, Ping Luo, Xiaogang Wang, and Xiaoou Tang. Large-scale celebfaces attributes (celeba) dataset. *Retrieved August, 15(2018):11*, 2018.
- [30] Maggie Makar, Ben Packer, Dan Moldovan, Davis Blalock, Yoni Halpern, and Alexander D’Amour. Causally motivated shortcut removal using auxiliary labels. In *International Conference on Artificial Intelligence and Statistics*, pages 739–766. PMLR, 2022.
- [31] Mazda Moayeri, Keivan Rezaei, Maziar Sanjabi, and Soheil Feizi. Text-to-concept (and back) via cross-model alignment. In *International Conference on Machine Learning*, pages 25037–25060. PMLR, 2023.
- [32] Nihal Murali, Aahlad Puli, Ke Yu, Rajesh Ranganath, and Kayhan Batmanghelich. Beyond distribution shift: Spurious features through the lens of training dynamics. *arXiv preprint arXiv:2302.09344*, 2023.
- [33] Jungho Nam et al. Learning from failure: Training debiased classifier from biased classifier. 2020.
- [34] Alec Radford, Jong Wook Kim, Chris Hallacy, Aditya Ramesh, Gabriel Goh, Sandhini Agarwal, Girish Sastry, Amanda Askell, Pamela Mishkin, Jack Clark, et al. Learning transferable visual models from natural language supervision. In *International conference on machine learning*, pages 8748–8763. PMLR, 2021.
- [35] Keivan Rezaei, Mehrdad Saberi, Mazda Moayeri, and Soheil Feizi. Prime: Prioritizing interpretability in failure mode extraction. *arXiv preprint arXiv:2310.00164*, 2023.

- [36] Svetlana Sagadeeva and Matthias Boehm. Sliceline: Fast, linear-algebra-based slice finding for ml model debugging. In *Proceedings of the 2021 International Conference on Management of Data*, pages 2290–2299, 2021.
- [37] Shiori Sagawa et al. Distributionally robust neural networks for group shifts: On the importance of regularization for worst-case generalization. 2020.
- [38] Sahil Singla, Besmira Nushi, Shital Shah, Ece Kamar, and Eric Horvitz. Understanding failures of deep networks via robust feature extraction. In *Proceedings of the IEEE/CVF Conference on Computer Vision and Pattern Recognition*, pages 12853–12862, 2021.
- [39] Nimit Sohoni, Jared Dunmon, Geoffrey Angus, Albert Gu, and Christopher Ré. No subclass left behind: Fine-grained robustness in coarse-grained classification problems. *Advances in Neural Information Processing Systems*, 33:19339–19352, 2020.
- [40] Mingxing Tan and Quoc Le. Efficientnet: Rethinking model scaling for convolutional neural networks. In *International conference on machine learning*, pages 6105–6114. PMLR, 2019.
- [41] Vladimir Vapnik. *The Nature of Statistical Learning Theory*. Springer, 1999.
- [42] Catherine Wah, Steve Branson, Peter Welinder, Pietro Perona, and Serge Belongie. The caltech-ucsd birds-200-2011 dataset. 2011.
- [43] Xiaosong Wang, Yifan Peng, Le Lu, Zhiyong Lu, Mohammadhadi Bagheri, and Ronald M Summers. Chestx-ray8: Hospital-scale chest x-ray database and benchmarks on weakly-supervised classification and localization of common thorax diseases. In *Proceedings of the IEEE conference on computer vision and pattern recognition*, pages 2097–2106, 2017.
- [44] Yuzhe Yang, Haoran Zhang, Dina Katabi, and Marzyeh Ghassemi. Change is hard: A closer look at subpopulation shift. *arXiv preprint arXiv:2302.12254*, 2023.
- [45] Yujia Yao et al. Learning invariant representations via continuous transformation networks. 2022.
- [46] Sriram Yenamandra, Pratik Ramesh, Viraj Prabhu, and Judy Hoffman. Facts: First amplify correlations and then slice to discover bias. In *IEEE/CVF International Conference in Computer Vision (ICCV)*, 2023.
- [47] Kihyun You, Jawook Gu, Jiyeon Ham, Beomhee Park, Jiho Kim, Eun K Hong, Woonhyuk Baek, and Byungseok Roh. Cxr-clip: Toward large scale chest x-ray language-image pre-training. In *International Conference on Medical Image Computing and Computer-Assisted Intervention*, pages 101–111. Springer, 2023.
- [48] Hongyi Zhang et al. mixup: Beyond empirical risk minimization. 2018.
- [49] Yuhui Zhang, Jeff Z HaoChen, Shih-Cheng Huang, Kuan-Chieh Wang, James Zou, and Serena Yeung. Diagnosing and rectifying vision models using language. In *International Conference on Learning Representations (ICLR)*, 2023. URL <https://openreview.net/pdf?id=D-zfUK7BR6c>.
- [50] Bolei Zhou, Agata Lapedriza, Aditya Khosla, Aude Oliva, and Antonio Torralba. Places: A 10 million image database for scene recognition. *IEEE Transactions on Pattern Analysis and Machine Intelligence*, 2017.

A Appendix / supplemental material

A.1 Broader impact

LADDER significantly impacts various sectors that rely on robust machine learning models, *e.g.*, healthcare, by providing a more transparent and accountable method for identifying and mitigating model errors. This approach is particularly pertinent given the increasing societal concern over the fairness and transparency of AI systems. By eliminating the need for explicit attribute annotations and utilizing naturally occurring language descriptions, LADDER democratizes the ability to audit and improve models, making these processes more accessible to non-experts and reducing the expertise barrier traditionally associated with model tuning.

A.2 Extended Limitation

One significant limitation of the LADDER is its reliance on the quality and comprehensiveness of the language data (either the captions or radiology report) used to generate hypotheses. While LADDER utilizes Large Language Models (LLMs) to interpret errors and generate hypotheses for error mitigation, the effectiveness of these hypotheses depends strongly upon the quality of the sentences. In scenarios where the sentences do not capture the domain-specific terminology, the quality of the generated hypotheses may be compromised. This can lead to suboptimal error slice discovery and might not fully capture the nuanced errors in specialized domains such as medical imaging or rare categories in natural images.

Another possible limitation is LADDER’s dependence on pretrained vision language models. If the vision language model does not align the images and languages, LADDER will struggle to generate proper hypotheses. Also, for domains with such vision language models that are nonexistent, LADDER’s applicability will be limited.

B Glossary of Terms and Notations

\mathcal{X}	Set of input images.
\mathcal{Y}	Set of labels.
X_Y	Set of images belonging to class label Y .
f	Trained classifier predicting class labels \mathcal{Y} from images \mathcal{X} .
g	Classification head of the model.
Φ	Image representation function of the classifier f .
Ψ^I, Ψ^T	Image and text encoders in the joint vision-language representation (VLR) space.
$\langle \cdot, \cdot \rangle$	Dot product operation, used to compute similarity scores between embeddings.
π	Projection function mapping image representations Φ to the VLR space Ψ^I .
Δ^I	Difference in mean of the projected representations of correctly and incorrectly classified samples.
t_{val}	Validation text corpus, such as radiology reports or image captions.
\mathcal{S}_Y	Error slices corresponding to class Y , <i>i.e.</i> , subset of images with class Y where the classifier f underperforms.
$\mathcal{S}_{Y, -\text{attr}}$	Ground truth error slice without attribute <code>attr</code> and class Y .
$e(\cdot)$	Error rate function for a given subset of data.
topK	topK sentences having highest similarity with Δ^I
\mathcal{H}	Set of hypotheses generated by LLM, each of which is an indicator of an attribute on which f may be biased.
\mathcal{T}	Set of sentences corresponding to test each of the set of hypotheses H .
\mathcal{T}_H	Set of sentence for the hypothesis $H \in \mathcal{H}$
s_H	Similarity score for a hypothesis H , measuring alignment of image representations with hypothesis-specific attributes.
$\mathcal{S}_{-H,Y}$	Subset of images for class Y not aligning with the hypothesis H , a potential candidate for an error slice.

\mathcal{R}

Retrieval function for selecting sentences with high similarity to ΔI .

τ

Threshold value for selecting images based on similarity scores for error slice identification.

B.1 Prompts used by LLM for hypotheses generation discussed in Sec. 2.2

RSNA Prompt

Context: Breast cancer classification from mammograms using a deep neural network

Analysis post-training: On a validation set,

- Get the difference between the image embeddings of correct and incorrectly classified samples to estimate the features present in the correctly classified samples but missing in the misclassified samples.
- Retrieve the top 100 sentences from the radiology report that match closely to the embedding difference in step a.
- The sentence list is given below:

top100 (topK) sentence list (retrieved using Sec. 2.1)

These sentences represent the features present in the correctly classified samples but missing in the misclassified samples.

Task: Ignore ‘___’ as they are due to anonymization. Consider the consistent attributes present in the descriptions of correctly classified and misclassified samples regarding positive cancer patients. Formulate hypotheses based on these attributes. Attributes are all the concepts (e.g., explicit or implicit anatomies, observations, any symptom of change related to the disease, demography-related information, or any concept leading to potential bias) in the sentences other than the class label (cancer in this case). Assess how these characteristics might be influencing the classifier’s performance. Your response should contain only the list of top hypotheses and nothing else. For the response, you should use the following Python dictionary template with no extra sentences:

```
hypothesis_dict =
{
  "H1": "The classifier is making mistake as it is biased toward <attribute>",
  "H2": "The classifier is making mistake as it is biased toward <attribute>",
  "H3": "The classifier is making mistake as it is biased toward <attribute>",
  ...
}
```

To effectively test Hypothesis1 (H1) using the CLIP language encoder, you must create prompts that explicitly validate H1. These prompts will help to generate text embeddings that capture the essence of the hypothesis, which can be used to compute similarity with the image embeddings from the dataset. The goal is to see if the images where the model makes mistakes align with H1 or violate H1. The prompts are a Python list. Remember, your focus is only on the class label "Cancer" (i.e, positive cancer cases)

Do this for all the hypotheses. Your final response should follow the following list of dictionaries, nothing else:

```
prompt_dict = {
  "H1_<attribute>": [List of prompts],
  "H2_<attribute>": [List of prompts],
  ...
}
```

Each attribute hypothesis should contain 5 prompts. So the final response should follow the below format strictly (nothing else, no extra sentence):

```
```python
```

```
hypothesis_dict
prompt_dict
...
```
```

Context: Pneumothorax classification from chest x-rays using a deep neural network

Analysis post-training: On a validation set,

- a. Get the difference between the image embeddings of correct and incorrectly classified samples to estimate the features present in the correctly classified samples but missing in the misclassified samples.
- b. Retrieve the top 100 sentences from the radiology report that match closely to the embedding difference in step a.
- c. The sentence list is given below:

top100 (topK) sentence list (retrieved using Sec. 2.1)

These sentences represent the features present in the correctly classified samples but missing in the misclassified samples.

Task: Ignore ‘___’ as they are due to anonymization. Consider the consistent attributes present in descriptions of correctly classified and misclassified samples regarding positive Pneumothorax patients. Formulate hypotheses based on these attributes. Attributes are all the concepts (e.g., explicit or implicit anatomies, observations, demography-related information, or any concept leading to potential bias) in the sentences other than the class label (Pneumothorax, in this case). Assess how these characteristics might be influencing the classifier’s performance. Your response should contain only the list of top hypotheses and nothing else. For the response, you should use the following Python dictionary template with no extra sentence:

```
hypothesis_dict =
{
  "H1": "The classifier is making mistake as it is biased toward <attribute>",
  "H2": "The classifier is making mistake as it is biased toward <attribute>",
  "H3": "The classifier is making mistake as it is biased toward <attribute>",
  ...
}
```

To effectively test Hypothesis1 (H1) using the CLIP language encoder, you must create prompts that explicitly validate H1. These prompts will help to generate text embeddings that capture the essence of the hypothesis, which can be used to compute similarity with the image embeddings from the dataset. The goal is to see if the images where the model makes mistakes are those that align with H1 or violate H1. The prompts are a python list. Remember, your focus is only on the class label "Pneumothorax" (i.e., positive Pneumothorax cases). Do this for all the hypotheses. Your final response should follow the following list of dictionaries, nothing else:

```
prompt_dict = {
  "H1_<attribute>": [List of prompts],
  "H2_<attribute>": [List of prompts],
  ...
}
```

Each attribute hypothesis should contain 5 prompts. So the final response should follow the below format strictly (nothing else, no extra sentence):

```
```python
hypothesis_dict
prompt_dict
```
```

Waterbirds Prompt

Context: Bird classification from images using a deep neural network

Analysis post-training: On a validation set,

- a. Get the difference between the image embeddings of correct and incorrectly classified samples to estimate the features present in the correctly classified samples but missing in the misclassified samples.
- b. Retrieve the top 200 sentences from the radiology report that match closely to the embedding difference in step a.
- c. The sentence list is given below:

top100 (topK) sentence list (retrieved using Sec. 2.1)

These sentences represent the features present in the correctly classified samples but missing in the misclassified samples.

Task: The task is to reason why the model makes mistakes on the misclassified samples based on the sentences. To do so, consider the attributes of the above captions regarding the specific bird species. Attributes are all the concepts other than the class label. So, develop a list of hypotheses based on these attributes to reason why a model makes systematic mistakes. For the hypotheses, you should use the following Python dictionary template, no extra sentences:

```
hypothesis_dict =
{
  "H1": "The classifier is making mistake as it is biased toward <attribute>",
  "H2": "The classifier is making mistake as it is biased toward <attribute>",
  "H3": "The classifier is making mistake as it is biased toward <attribute>",
  ...
}
```

You must follow the following rules to construct the hypotheses:

1. You must pick specific attributes, e.g, blue, not generic attributes like color.
2. Your hypotheses must be based on the attributes present in the captions, nothing else.
3. You must pay close attention to the attributes consistently in the sentences. These attributes are likely to cause systematic mistakes in the misclassified samples.
4. You must construct as many hypotheses as possible.

Next, you have to test the hypothesis. To effectively test Hypothesis1 (H1) using the CLIP language encoder, you must create prompts that explicitly validate H1. These prompts will help to generate text embeddings that capture the essence of the hypothesis, which can be used to compute similarity with the image embeddings from the dataset. The goal is to see if the images for which the model makes mistakes align with H1 or violate H1. The prompts are a Python list. Remember, your focus is only on the specific bird.

Do this for all the hypotheses. Your final response should follow the following list of dictionaries, nothing else:

```
prompt_dict = {
  "H1_<attribute>": [List of prompts],
  "H2_<attribute>": [List of prompts],
  ...
}
```

Each attribute hypothesis should contain 5 prompts. So the final response should follow the below format strictly (nothing else, no extra sentence):

```
```python
```

```
hypothesis_dict
prompt_dict
```
```

CelebA Prompt

Context: Hair color (Blonde/Non blonde) classification from images of men and women using a deep neural network

Analysis post-training: On a validation set,

- a. Get the difference between the image embeddings of correct and incorrectly classified samples to estimate the features present in the correctly classified samples but missing in the misclassified samples.
- b. Retrieve the top 200 sentences from the radiology report that match closely to the embedding difference in step a.
- c. The sentence list is given below:

top100 (topK) sentence list (retrieved using Sec. 2.1)

These sentences represent the features present in the correctly classified samples but missing in the misclassified samples.

Task: The task is to reason why the model makes mistakes on the misclassified samples based on the sentences. To do so, consider the attributes present in the above captions regarding the samples with Blonde hair (i.e., the class label "Blonde"). Attributes are all the concepts (e.g., demography-related concepts, etc.) other than the class label. For example, key attributes to consider in the first sentence are woman, long hair, smiling, and black top. So, develop a list of hypotheses based on these attributes to explain why a model makes systematic mistakes. For the hypotheses, you should use the following Python dictionary template, with no extra sentence:

```
hypothesis_dict =
{
  "H1": "The classifier is making mistake as it is biased toward <attribute>",
  "H2": "The classifier is making mistake as it is biased toward <attribute>",
  "H3": "The classifier is making mistake as it is biased toward <attribute>",
  ...
}
```

You must follow the following rules to construct the hypotheses:

1. You must pick specific attributes, e.g, white dress, not generic attributes like dress color.
2. Your hypotheses must be based on the attributes present in the captions, nothing else.
3. You must pay close attention to the attributes consistently in the sentences. These attributes are likely to cause systematic mistakes in the misclassified samples.
4. You must construct as many hypotheses as possible.

Next, you have to test the hypothesis. To effectively test Hypothesis1 (H1) using the CLIP language encoder, you must create prompts that explicitly validate H1. These prompts will help to generate text embeddings that capture the essence of the hypothesis, which can be used to compute similarity with the image embeddings from the dataset. The goal is to see if the images for which the model makes mistakes align with H1 or violate H1. The prompts are a Python list. Remember, your focus is only on the class label "Blonde" (i.e, men/women with Blonde hair)

Do this for all the hypotheses. Your final response should follow the following list of dictionaries, nothing else:

```
prompt_dict = {
  "H1_<attribute>": [List of prompts],
  "H2_<attribute>": [List of prompts],
  ...
}
```

Each attribute hypothesis should contain 5 prompts. So the final response should follow the below format strictly (nothing else, no extra sentence):

```
```python
hypothesis_dict
prompt_dict
```
```

MetaShift Prompt

Context: Cat vs Dog classification from images using a deep neural network

Analysis post-training: On a validation set,

- a. Get the difference between the image embeddings of correct and incorrectly classified samples to estimate the features present in the correctly classified samples but missing in the misclassified samples.
- b. Retrieve the top 200 sentences from the radiology report that match closely to the embedding difference in step a.
- c. The sentence list is given below:

top100 (topK) sentence list (retrieved using Sec. 2.1)

These sentences represent the features present in the correctly classified samples but missing in the misclassified samples.

Task: The task is to reason why the model makes mistakes on the misclassified samples based on the sentences for the class label “<class label>”. To do so, consider the attributes present in the above captions regarding to the specific bird species. Attributes are all the concepts other than the class label (i.e, "<class label>"). So, develop a list of hypotheses based on these attributes to reason why a model makes systematic mistakes. For the hypotheses, you should use the following Python dictionary template, with no extra sentence:

```
hypothesis_dict =
{
  "H1": "The classifier is making mistake as it is biased toward <attribute>",
  "H2": "The classifier is making mistake as it is biased toward <attribute>",
  "H3": "The classifier is making mistake as it is biased toward <attribute>",
  ...
}
```

You must follow the following rules to construct the hypotheses:

1. You must pick specific attributes, e.g, blue, not generic attributes like color.
2. Your hypotheses must be based on the attributes present in the captions, nothing else.
3. You must pay close attention to the attributes consistently in the sentences. These attributes are likely to cause systematic mistakes in the misclassified samples.
4. You must construct as many hypotheses as possible.

Next, you have to test the hypothesis. To effectively test Hypothesis1 (H1) using the CLIP language encoder, you must create prompts that explicitly validate H1. These prompts will help to generate text embeddings that capture the essence of the hypothesis, which can be used to compute similarity with the image embeddings from the dataset. The goal is to see if the images for which the model makes mistakes are those that align with H1 or violate H1. The prompts are a Python list. Remember, your focus is only on the specific bird.

Do this for all the hypotheses. Your final response should follow the following list of dictionaries, nothing else:

```
prompt_dict = {
  "H1_<attribute>": [List of prompts],
  "H2_<attribute>": [List of prompts],
  ...
}
```

Each attribute hypothesis should contain 5 prompts. So the final response should follow the below format strictly (nothing else, no extra sentence):

```
```python
```

```
hypothesis_dict
prompt_dict
```
```

B.2 Extended details on datasets

Waterbirds

The *Waterbirds* dataset [42] is frequently employed in studies addressing spurious correlations. This binary classification dataset overlaps images from the Caltech-UCSD Birds-200-2011 (CUB) dataset with backgrounds sourced from the Places dataset [50]. The primary task involves determining whether a bird depicted in an image is a landbird or a waterbird, with the background (water or land) as the spurious attribute. For consistency and comparability, we adhere to the train/validation/test splits utilized in prior research [13].

CelebA

The *CelebA* dataset [28] comprises over 200,000 images of celebrity faces. In the context of spurious correlations research, this dataset is typically used for the binary classification task of predicting hair color (blond vs. non-blond), with gender serving as the spurious correlation. In alignment with previous studies [13], we use the standard dataset splits. The CelebA dataset is available under the Creative Commons Attribution 4.0 International license.

MetaShift

The *MetaShift* dataset [25] offers a flexible platform for generating image datasets based on the Visual Genome project [20]. Our experiments utilize the pre-processed *Cat vs. Dog* dataset, designed to differentiate between cats and dogs. The dataset features the image background as a spurious attribute, with cats typically appearing indoors and dogs outdoors. We use the "unmixed" version of this dataset, as provided by the authors' codebase.

NIH chestXrays

The *NIH ChestX-ray* dataset [43], also known as ChestX-ray14, is a large dataset of chest radiographs (X-rays) provided by the National Institutes of Health (NIH). The dataset comprises 112,120 frontal-view X-ray images of 30,805 unique patients. Each image is associated with one or more of the 14 labeled thoracic diseases, which include atelectasis, cardiomegaly, effusion, infiltration, mass, nodule, pneumonia, pneumothorax, consolidation, edema, emphysema, fibrosis, pleural thickening, and hernia. Previous works [8] show that most pneumothorax patients have a spurious correlation with the chest drains. Chest drains are used to treat positive Pneumothorax cases. We adopt the strategy discussed in [32] to annotate chest drains for each sample. We use the official train/val/test split [43].

RSNA breast mammograms

The *RSNA-Mammo*⁴ is a publicly available dataset having 11913 patients with 486 cancer cases. The aim is to classify malignant patients from screening mammograms. We use train/val/test split as 0.7/0.2/0.1.

B.3 Extended details on slice discovery algorithms

Domino. Domino identifies systematic errors in machine learning models by leveraging cross-modal embeddings. It operates in three main steps: embedding, slicing, and describing.

1. **Embedding:** Domino uses cross-modal models (*e.g.*, CLIP) to embed inputs and text in the same latent space. This enables the incorporation of semantic meaning from text into input embeddings, which is crucial for identifying coherent slices.
2. **Slicing:** It employs an error-aware mixture model to detect underperforming regions within the embedding space. This model clusters the data based on embeddings, class labels, and model predictions to pinpoint areas where the model performance is subpar. The mixture model ensures that identified slices are coherent and relevant to model errors.

⁴<https://www.kaggle.com/competitions/rsna-breast-cancer-detection>

3. **Describing:** Domino generates natural language descriptions for the discovered slices. It creates prototype embeddings for each slice and matches them with text embeddings to describe the common characteristics of the slice. This step provides interpretable insights into why the model fails on these slices.

Domino’s approach improves slice coherence and generates meaningful slice descriptions.

FACTS. FACTS (First Amplify Correlations and Then Slice) aims to identify bias-conflicting slices in datasets through a two-stage process:

1. **Amplify Correlations:** This stage involves training a model with a high regularization term to amplify its reliance on spurious correlations present in the dataset. This step helps segregate biased-aligned from bias-conflicting samples by making the model fit a simpler, biased-aligned hypothesis.
2. **Correlation-aware Slicing:** In this stage, FACTS uses clustering techniques on the bias-amplified feature space to discover bias-conflicting slices. The method identifies subgroups where the spurious correlations do not hold, highlighting areas where the model underperforms due to these biases.

FACTS leverages a combination of bias amplification and clustering to reveal underperforming data slices, providing a foundation for understanding and mitigating systematic biases in machine learning models.

B.4 Extended details on error mitigation baselines

We categorize the various bias mitigation algorithms and provide detailed descriptions for each category below.

Vanilla

The empirical risk minimization (ERM) algorithm, introduced by Vapnik [41], seeks to minimize the cumulative error across all samples.

Subgroup Robust Methods

GroupDRO: GroupDRO [37] propose Group Distributionally Robust Optimization (GroupDRO), which enhances ERM by prioritizing groups with higher error rates. **CVaRDRO:** Duchi and Namkoong [9] introduce a variant of GroupDRO that dynamically assigns weights to data samples with the highest losses. **LfF:** LfF [33] concurrently trains two models: the first model is biased, and the second is de-biased by re-weighting the loss gradient. **Just Train Twice (JTT):** JTT [27] propose an approach that initially trains an ERM model to identify minority groups in the training set, followed by a second ERM model where the identified samples are re-weighted. **LISA:** LISA [45] utilizes invariant predictors through data interpolation within and across attributes. **Deep Feature Re-weighting (DFR):** DFR [14] suggests first training an ERM model and then retraining the final layer using a balanced validation set with group annotations.

Data Augmentation

Mixup: Mixup [48] proposes an approach that performs ERM on linear interpolations of randomly sampled training examples and their corresponding labels.

Domain-Invariant Representation Learning

Invariant Risk Minimization (IRM): IRM [2] learns a feature representation such that the optimal linear classifier on this representation is consistent across different domains. **Maximum Mean Discrepancy (MMD):** MMD [23] utilizes MMD [11] to match feature distributions across domains. **Note:** All methods in this category necessitate group annotations during training.

Imbalanced Learning

Focal Loss (Focal): Focal [26] introduces Focal Loss, which reduces the loss for well-classified samples and emphasizes difficult samples. **Class-Balanced Loss (CBLoss):** CBLoss [6] suggests re-weighting by the inverse effective number of samples. **LDAM Loss (LDAM):** LDAM [3] employs a modified margin loss that preferentially weights minority samples. **Classifier Re-training (CRT):** CRT [17] decomposes representation learning and classifier training into two distinct stages, re-weighting the classifier using class-balanced sampling during the second stage. **ReWeightCRT:** ReWeightCRT [17] proposes a re-weighted variant of CRT.

B.5 Algorithm of our proposed slice discovery

Algorithm 1 Hypothesis-driven Error Slice Detection

- 1: **Input:** $f = g \circ \Phi$: trained classifier, t_{val} : text corpus, $\{\Psi^I, \Psi^T\}$: image and text encoders of VLR space, \mathcal{X}_Y : images with class Y , N : number of images for balancing
 - 2: **Output:** Mitigated classifier f
 - 3: **Step 1: Retrieve Sentences Signifying Error**
 - 4: Learn projection function $\pi : \Phi \rightarrow \Psi^I$
 - 5: Compute $\Delta^I = \mathbb{E}_{X,Y|f(X)=Y}[\pi(\Phi(X))] - \mathbb{E}_{X,Y|f(X)\neq Y}[\pi(\Phi(X))]$
 - 6: Retrieve topK sentences using Sec. 2.1.
 - 7: **Step 2: Hypothesis Generation via LLM**
 - 8: Construct prompt with topK sentences based on Sec. B.1
 - 9: Generate hypotheses \mathcal{H} and testing sentences \mathcal{T} : $\{\mathcal{H}, \mathcal{T}\} = \text{LLM}(\text{prompt}, \text{topK})$
 - 10: **Step 3: Discover Error Slices**
 - 11: **for** each hypothesis $H \in \mathcal{H}$ **do**
 - 12: Compute mean text embedding: $\Psi^T(\mathcal{T}_H) = \frac{1}{|\mathcal{T}_H|} \sum_{t \in \mathcal{T}_H} \Psi^T(t)$
 - 13: **for** each image $X \in \mathcal{X}_Y$ **do**
 - 14: Project image to VLR space: $\pi(\Phi(X))$
 - 15: Compute similarity score using Eq. 1
 - 16: **end for**
 - 17: Identify error slice: $\mathcal{S}_{Y,-H} = \{X \in \mathcal{X}_Y \mid s_H(X) < \tau\}$
 - 18: **if** $e(\mathcal{S}_{Y,-H}) \gg e(\mathcal{X}_Y)$ **then**
 - 19: Add $\mathcal{S}_{Y,-H}$ to $\hat{\mathcal{S}}_Y$
 - 20: **end if**
 - 21: **end for**
-

B.6 Pytorch-style code

B.6.1 Stage 1: Retrieve Sentences Signifying Error

```
1 # Load CLIP model
2 clip_model = ...
3 clip_processor = ...
4
5 # Define functions for projections and similarity
6 def project_to_vlr_space(image_features):
7     return clip_model.get_image_features(image_features)
8
9 def compute_similarity(image_emb, text_emb):
10    return torch.matmul(image_emb, text_emb.T)
11
12 # Retrieve topK sentences
13 def retrieve_topk_sentences(diff_embedding, text_corpus, top_k=K):
14    text_inputs = clip_processor(text=text_corpus, return_tensors="pt", padding=True
15    )
16    text_embeddings = clip_model.get_text_features(**text_inputs)
17    similarities = compute_similarity(diff_embedding, text_embeddings)
18    topk_indices = similarities.topk(top_k).indices
19    return [text_corpus[i] for i in topk_indices]
20
21 # Example usage
22 diff_embedding = ...
23 val_text_corpus = ...
24 topk_sentences = retrieve_topk_sentences(diff_embedding, val_text_corpus)
```

B.6.2 Stage 1: Retrieve Sentences Signifying Error

```
1 def get_hypothesis_from_LLM(open_ai_key, prompt, hypothesis_dict_file,
2   prompt_dict_file):
3   openai.api_key = open_ai_key
4   headers = {
5       "Content-Type": "application/json",
6       "Authorization": f"Bearer {openai.api_key}"
7   }
8
9   payload = {
10      "model": "gpt-4-turbo",
11      "messages": [
12          {
13              "role": "user",
14              "content": [
15                  {
16                      "type": "text",
17                      "text": prompt
18                  }
19              ]
20          },
21          {
22              "max_tokens": 3000,
23              "temperature": 0.5,
24              "seed": 42
25          }
26      ]
27
28      response = requests.post("https://api.openai.com/v1/chat/completions", headers=
29        headers, json=payload)
30      data = response.json()
31      clean_python_code = data["choices"][0]["message"]["content"].strip("`").split("
32        python\n")[1]
33      local_vars = {}
34      exec(clean_python_code, {}, local_vars)
35
36      hypothesis_dict = local_vars["hypothesis_dict"]
37      prompt_dict = local_vars["prompt_dict"]
38
39      # Save these dictionaries
40
41  # Example usage
42  open_ai_key = ...
43  prompt = ...
44  hypotheses, prompts = get_hypothesis_from_LLM(open_ai_key, prompt,
45    hypothesis_dict_file, prompt_dict_file)
```

B.6.3 Stage 3: Mitigate Errors without Annotation

```
1 def create_balanced_dataset(images, labels, similarity_scores, top_n):
2     high_sim_indices = similarity_scores.topk(top_n, largest=True).indices
3     low_sim_indices = similarity_scores.topk(top_n, largest=False).indices
4     balanced_indices = torch.cat([high_sim_indices, low_sim_indices])
5     return images[balanced_indices], labels[balanced_indices]
6
7 # Mitigate errors
8 def mitigate_errors(images, labels, hypotheses, similarity_scores, strategy="
9     seq_tune", top_n=50):
10    if strategy == "slice_info":
11        best_hypothesis = max(hypotheses, key=lambda h: compute_similarity(h, "
12            attribute")) # Example attribute
13        balanced_images, balanced_labels = create_balanced_dataset(images, labels,
14            similarity_scores, top_n)
15        fine_tune_classifier(balanced_images, balanced_labels) # Define this
16            function as per your model
17
18    elif strategy == "seq_tune":
19        for hypothesis in hypotheses:
20            balanced_images, balanced_labels = create_balanced_dataset(images, labels
21                , similarity_scores, top_n)
22            fine_tune_classifier(balanced_images, balanced_labels)
23
24    elif strategy == "ensemble":
25        classifiers = []
26        for hypothesis in hypotheses:
27            balanced_images, balanced_labels = create_balanced_dataset(images, labels
28                , similarity_scores, top_n)
29            classifier = fine_tune_classifier(balanced_images, balanced_labels)
30            classifiers.append(classifier)
31        return classifiers # Ensemble these classifiers during inference
32
33 # Example usage
34 train_images = ...
35 train_labels = ...
36 hypotheses = ...
37 similarity_scores = ...
38 mitigate_errors(train_images, train_labels, hypotheses, similarity_scores, strategy="
39     seq_tune")
```

B.7 Extended details on experiments

B.7.1 Vision Language embedding of Mammograms

We develop a CLIP model using an in-house mammography dataset from a US-based hospital using De-CLIP [22] loss. **Pre-processing the images.** We use a rule-based approach to find the breast's ROI for all the datasets. We set values less than 40 to 0 and eliminate the consistently identical rows and columns, as they denote the background. It results in images with an average aspect ratio of 1:1.6 to 2, finally resized to 1520×912 . **Pre-training.** For text encoding, we deploy BioClinicalBERT, while EfficientNet B5 with pre-trained ImageNet weights serves as our image encoder. We augment the images via affine transformations—rotations up to 20° , translations starting from 0.1%, scaling between 0.8 and 1.2, and shearing up to 20° —and elastic transformations characterized by $\alpha = 10$ and $\sigma = 5$. Text augmentation strategies include sentence swaps and back-translations from Italian to English. We train the model for 10 epochs using mixed-precision techniques, optimizing with AdamW at an initial rate of $5e-5$ and a decay of $1e-4$. A cosine-annealing scheduler with a single-epoch warm-up manages the learning rate adjustments.

B.7.2 Implementation details of the source model f using ERM

We train imagenet-pretrained ResNet-50 model [12] as f for natural images and NIH-CXR as described in [44]. We use the codebase⁵ to train the models for natural images. We preprocess the images by resizing and center cropping the image to 224×224 pixels and normalizing the image using the ImageNet channel statistics. Following previous research [13, 14], we apply SGD with momentum to all image datasets. For convergence, we train every model for 30,000 steps across all datasets, divided into 5,000 steps on Waterbirds and MetaShift. For NIH-CXR, we use Adam optimizer with a learning rate of 0.0001 and train it for 60 epochs. For RSNA-Mammo, we use the codebase⁶, one of the leaders in the kaggle competition. Specifically, we resize the images to 1520×912 and train an efficient net B5 [40] model for 9 epochs using SGD optimizer with a learning rate of $5e-5$ and weight decay of $1e-4$. For CXR-CLIP, we utilize their pre-trained models⁷.

B.7.3 Implementation Details of the projection model π

For the projection π aligning the representation of classifier with image embedding in the VLR space, we utilize the aligner discussed in [31] (using the open source codebase⁸) to train a single layer neural network using SGD optimizer with a learning rate of 0.01. We optimize the model for 30, 200, and 30 epochs for natural images, NIH-CXR, and RSNA-Mammo.

B.8 Computing resources

All the models are implemented in PyTorch and trained on a single NVIDIA RTX-6000 GPU with 32G of memory. We use the checkpoints from the official repository of CLIP and CXR-CLIP. The vision language pretrained model for mammograms takes 36 hours to train. Classifiers trained with natural images take 8 hours to train. The Classifier with NIH-CXR takes approximately 15 hours to train. The Classifier with RSNA-Mammo takes approximately 15 hours to train.

B.9 Extended results

B.9.1 Language as an alternative to attributes to analyze the errors

In this experiment, we ask this fundamental question, “can language be used as an alternative to discover the slices?” As illustrated in Table 3, utilizing caption embeddings instead of explicit attributes achieves comparable RMSE for predicting model errors on CelebA and Waterbirds datasets. The strong Spearman and Pearson correlation coefficients between model errors predicted by language embeddings and biased attributes suggest that language effectively captures bias patterns, providing a reliable proxy for ground truth attributes.

Table 3: Comparison of RMSE and correlation coefficients for model error prediction using attributes and caption embeddings

| Dataset | RMSE
w/ attributes | RMSE
w/ caption embeddings | Spearman | Pearson |
|------------|-----------------------|-------------------------------|----------|---------|
| Waterbirds | 6.7311 | 6.6906 | 0.6159 | 0.5204 |
| CeleA | 2.0753 | 2.0677 | 0.7119 | 0.6497 |

B.9.2 Statistical Significance

To statistically validate the performance of subsets in line with the hypotheses generated by the language model, we conduct t-tests across various hypotheses. We compare the observed accuracies of subsets where the hypothesized attributes are present to a null distribution designed to reflect a scenario where these attributes do not affect the classifier’s accuracy.

For each hypothesis, we sample subsets from our dataset where the specific attribute mentioned in the hypothesis is present. This allows us to compute the mean observed accuracy for images exhibiting attributes relevant to each hypothesis. To construct a null distribution, we randomly sample an equal number of images, both with and without the attribute. This balanced sampling approach is crucial

⁵<https://github.com/YyzHarry/SubpopBench>

⁶<https://github.com/Masaaaato/RSNABreast7thPlace>

⁷<https://github.com/kakaobrain/cxr-clip>

⁸<https://github.com/k1rezaei/Text-to-concept/tree/main>

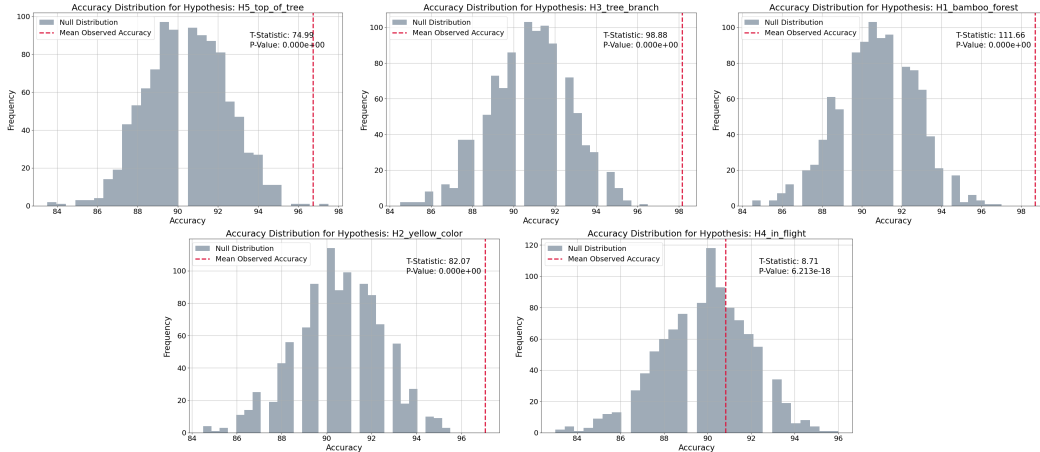


Figure 5: Statistical validation of hypotheses on the biases of RN50-based classifier for *landbird* classification of Waterbirds dataset. Each panel represents a hypothesis tested, displaying the observed accuracy distribution against a null distribution. The t-statistics and p-values indicate significant differences, supporting the hypothesis that the presence of specific attributes significantly affects model accuracy.

as it simulates the null hypothesis scenario that the attribute does not influence the classification accuracy.

The experiment is conducted with 1000 iterations for each hypothesis. In each iteration, 100 data points are randomly selected to calculate the classification accuracy against the ground truth. This repetitive sampling ensures robustness in our statistical testing by accurately approximating the distribution of accuracies under both observed and null conditions.

We apply a t-test (using `ttest_ind` from the `scipy.stats` package) for each hypothesis to compare the mean accuracies of the observed and null distributions. The t-test, chosen for its suitability in comparing means from two independent samples, provides a t-statistic and a p-value. These statistics quantify the evidence against the null hypothesis, offering a measure of the impact of the hypothesized attribute on model performance.

In our study, we utilize the RN50 model across various datasets, including Waterbirds, CelebA, NIH-CXR, and RSNA-Mammo, to evaluate the impact of identified attributes in each hypothesis on classification accuracy. Figures 6, 5, 7, 9, and 8 depict the t-test results for each dataset respectively.

Across all datasets, we observe consistently large t-statistics and extremely low p-values. This consistent pattern provides robust statistical evidence supporting the hypothesis that the attributes identified by LLM significantly influence the model’s performance. The identified attributes, hypothesized by the LLM, correspond closely with the true underlying attributes that exhibit bias in the classifier f .

For each hypothesis, the observed mean accuracies in subsets of data where these attributes are present significantly exceeded those where these attributes were absent, as illustrated by the distinct separation in the distributions shown in the figures. This validation confirms that these attributes are critical for achieving higher classification accuracy and that their proper identification and incorporation into model training can substantially reduce biases and improve the overall performance of the classifier.

B.9.3 Impact of different vision language models on the retrieval of sentences and hypothesis generation

Fig 10 compares the sentences retrieved in Sec. 2.1, signifying the attributes present in the correctly classified samples but missing in the misclassified samples. We perform this experiment using CXR-CLIP as VLR space pretrained with the MIMIC-CheXpert-ChestX-ray14 (MCC) and MIMIC-CheXpert (MC) datasets, respectively and retrieve top500 sentences. Also, Fig. 11 shows the hypothesis generated by LLM using the sentences retrieved using the two variants of CXR-CLIP.

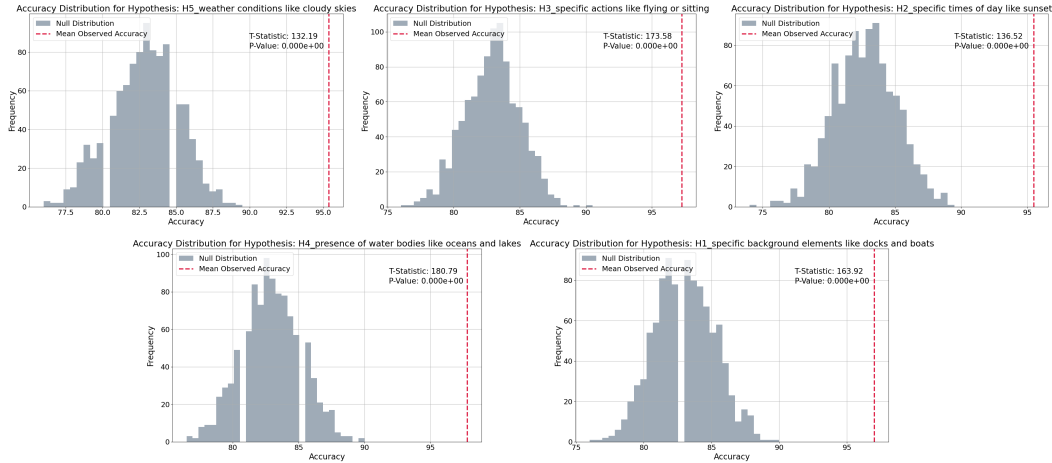


Figure 6: Statistical validation of hypotheses on the biases of RN50-based classifier for *waterbird* classification of Waterbirds dataset. Each panel represents a hypothesis tested, displaying the observed accuracy distribution against a null distribution. The t-statistics and p-values indicate significant differences, supporting the hypothesis that the presence of specific attributes significantly affects model accuracy.

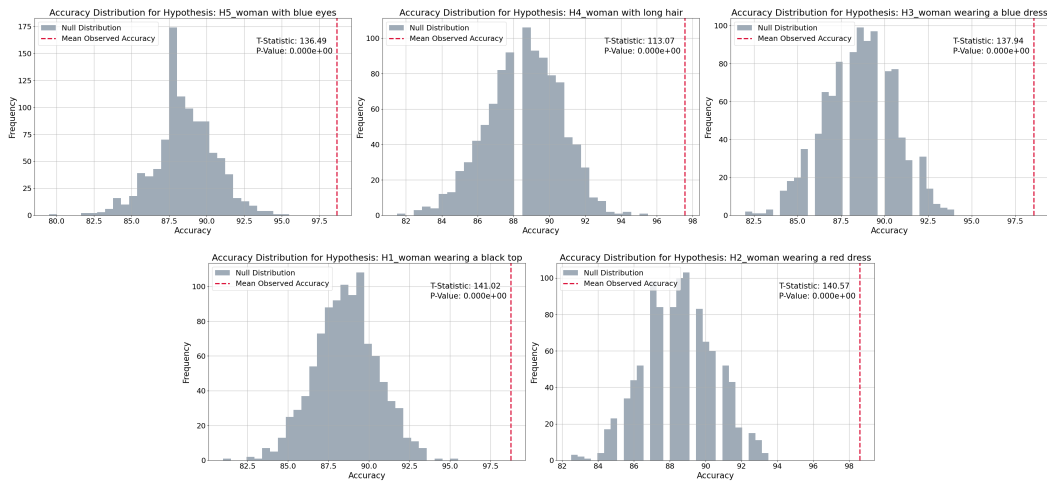


Figure 7: Statistical validation of hypotheses on the biases of RN50-based classifier for *blond* classification of CelebA dataset. Each panel represents a hypothesis tested, displaying the observed accuracy distribution against a null distribution. The t-statistics and p-values indicate significant differences, supporting the hypothesis that the presence of specific attributes significantly affects model accuracy.

We observe that in both cases, the hypotheses identify chest tube or chest drain as a source of bias. Also, in both cases, the size and types of pneumothorax are highlighted. Notably, the MCC variant shows a substantially higher count of “chest tube” mentions, with 268 instances compared to the 114 mentions recorded by the MC variant (Fig. 12). This discrepancy highlights the influence of dataset composition and pretraining on our framework’s ability to detect clinical attributes associated with pneumothorax in CXRs. The MCC variant integrates ChestX-ray14 data during the pertaining stage. So, it includes a broader variety of chest tube-related images. This experiment shows that the vision language model influences the formulation of the hypotheses.

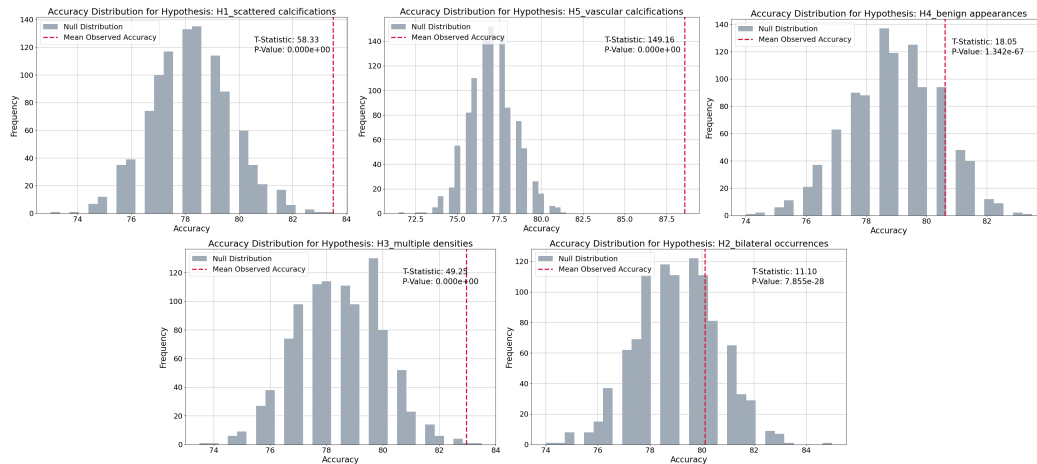


Figure 8: Statistical validation of hypotheses on the biases of classifier for *cancer* classification of the RSNA-Mammo dataset. Each panel represents a hypothesis tested, displaying the observed accuracy distribution against a null distribution. The t-statistics and p-values indicate significant differences, supporting the hypothesis that the presence of specific attributes significantly affects model accuracy.

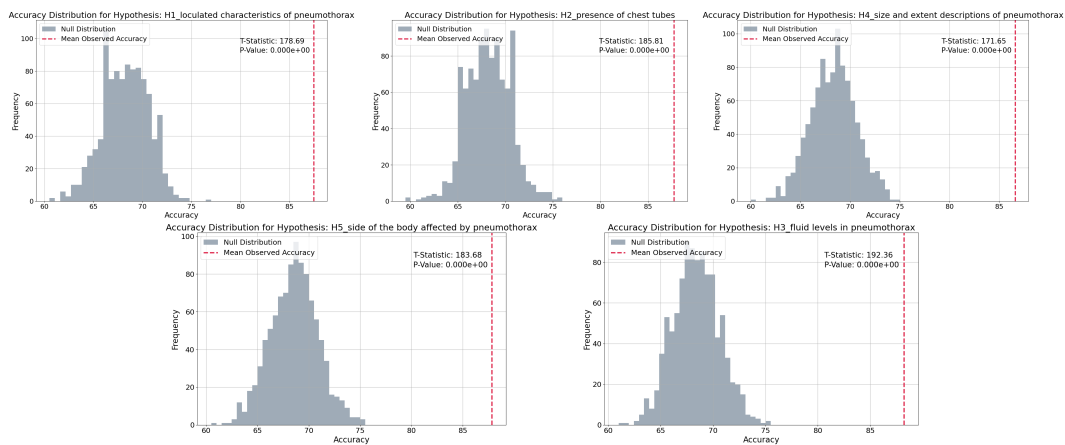


Figure 9: Statistical validation of hypotheses on the biases of RN50-based classifier for *pneumothorax* classification of NIH-CXR dataset. Each panel represents a hypothesis tested, displaying the observed accuracy distribution against a null distribution. The t-statistics and p-values indicate significant differences, supporting the hypothesis that the presence of specific attributes significantly affects model accuracy.

| Sentences indicating the biased attributes using CXR-CLIP (M,C,C) | Sentences indicating the biased attributes using CXR-CLIP (M,C) |
|---|--|
| <p>1. interval placement of right apical and right base pleural drains with slight decrease in right hydropneumothorax</p> <p>2. on ____, patient had right thoracotomy and two apical and a basal pleural drains were placed and there was a substantial decrease in the volume of homogeneous opacity in the right upper chest, presumably hematoma</p> <p>3. two chest tubes remain in place in the right hemithorax with a persistent moderate to large right pneumothorax with apical pneumothorax component and basilar hydropneumothorax</p> <p>4. two right chest tubes remain in place, with persistent moderate right pneumothorax, including apical pneumothorax component and basilar hydropneumothorax component</p> <p>5. interval increase in size of the small right - sided pneumothorax with chest tube in place</p> <p>6. moderate right pneumothorax despite the presence of three right chest tubes</p> <p>7. in comparison with the study of ____, there is been a right middle lobectomy with 2 chest tubes in place and substantial pneumothorax</p> <p>8. in comparison with study of ____, there are now two chest tubes in place on the right with a small pneumothorax</p> <p>9. right chest tubes remain in place, with persistent moderate - to - large right pneumothorax with apical pneumothorax component and basilar hydropneumothorax</p> <p>10. extensive surgical changes are observed in the right lung with surgical sutures and three chest tubes, one apically and two basilarly located</p> <p>11. interval placement of a chest tube with a somewhat loculated pneumothorax in the right apex and the lateral lung in the area of recent surgery</p> <p>12. increase in right apical pneumothorax with two chest tubes in place and no evidence of tension</p> <p>13. in comparison with the earlier study of this date, there has been a small increase in the substantial right apical and basilar pneumothorax with the chest tube on water seal</p> <p>14. in comparison with the study of ____, there again is evidence of previous right upper lobectomy with two chest tubes in place and persistent pneumothorax</p> <p>15. ap chest compared to __ through __, 4 : 45 p . m . : moderate - to - large right pneumothorax improved between __ and __ and has been stable all day, despite presence of two right pleural tubes ending in the upper hemithorax</p> <p>16. interval increase in size of a moderate to large right pneumothorax with the chest tubes on water seal</p> <p>17. interval insertion of a right - sided chest tube in good position, right - sided hydro pneumothorax has changed with increased pleural air are and relative decrease of the pleural fluid</p> <p>18. of the placing the left chest tube on water seal, there is a minimal increase in extent of the left postoperative predominantly basal pneumothorax</p> | <p>1. perhaps mild increase in hydropneumothorax but with chest tube remaining in place and no striking change</p> <p>2. in comparison with the study of ____, there is little change in the 3 left chest tubes with area of hydro pneumothorax persisting in the lateral aspect of the upper left chest as well as probably the left lung base</p> <p>3. a moderate sized loculated hydropneumothorax demonstrates decrease in fluid component and increasing gas component, particularly in the right base</p> <p>4. small right pleural effusion has replaced the previous basal pneumothorax that developed with previous drainage of pleural effusion and placement of 2 thoracostomy tubes</p> <p>5. 2 right indwelling pleural drains are unchanged in their respective positions, and there has probably been some decrease in the volume of the right posterior air and pleural collection in the rib right lower hemi thorax</p> <p>6. interval placement of right apical and right base pleural drains with slight decrease in right hydropneumothorax</p> <p>7. other less likely possibility include expansion of known loculated hydropneumothorax (chest tube does not appear to be draining this region)</p> <p>8. increasing fluid within the multiple pockets of the pneumothorax on the right</p> <p>9. decreased fluid and increased air in the right basilar hydropneumothorax, where the pleural catheter resides</p> <p>10. moderate right pleural effusion with loculated hydro pneumothorax components is again demonstrated, with apparent slight increase in extent of right basilar hydro pneumothorax</p> <p>11. three right - sided chest tubes remain in place with decrease in the loculated basilar hydropneumothoraces and some interval improvement in aeration at the right base</p> <p>12. loculated right hydro pneumothorax, with right basilar pneumothorax component slightly increased</p> <p>13. the only change is increasing fluid within a loculated hydropneumothorax, with corresponding decrease in air, located along the left lateral chest wall, of uncertain significance in the short - term postoperative course</p> <p>14. multiple small loculated hydropneumothoraces are again demonstrated, with interval worsening of loculated hydropneumothoraces at the left base</p> <p>15. fluid has now replaced air in the lateral component of the multi loculated left hydro pneumothorax, despite the insertion in that location of a new small drainage catheter</p> <p>16. loculated he mall / hydro pneumothorax in the upper portion of the chest as well as in the left lung base are unchanged</p> <p>17. small - to - moderate right hydropneumothorax, increase in the lateral costal fluid collection, and stable small apical air component</p> <p>18. successful placement of chest tube and pleura tube, small right basal loculated pneumothorax replaces area of successful pleural drainage</p> |

Figure 10: Comparing attribute identification using languages using different variants of CXR-CLIP Models. M, C, and C14 denote MIMIC-CXR, CheXpert, and ChestX-ray14, respectively. The left panel displays sentences retrieved from the MCC variant, while the right panel shows sentences from the MC variant. Both identify key attributes such as chest tubes and pneumothorax characteristics, with notable differences in the frequency of mentions, reflecting the impact of vision language pretrained models in identifying clinical features.

| Hypotheses with from sentences generate from CXR-CLIP (M,C,C) | Hypotheses with from sentences generate from CXR-CLIP (M,C) |
|---|--|
| <p>Hypotheses:</p> <p>The classifier is making mistake as it is biased toward:</p> <p>H1: chest tubes</p> <p>H2: apical components</p> <p>H3: descriptions of basilar components</p> <p>H4: subcutaneous emphysema</p> <p>H5: size descriptors of pneumothorax (small, moderate, large)</p> <p>Prompt to test each hypotheses:</p> <p>1. H1_chest_tubes: ['Chest x-ray showing pneumothorax with chest tubes in place.', 'Image of a lung with pneumothorax and visible chest tubes.', 'Chest radiograph of pneumothorax managed with chest tubes.', 'Diagnostic image displaying pneumothorax with chest tubes inserted.', 'Clinical chest x-ray with pneumothorax featuring chest tubes.']</p> <p>2. H2_apical_components: ['Chest x-ray showing pneumothorax with apical component.', 'Image of a lung with pneumothorax affecting the apex.', 'Chest radiograph of pneumothorax with apical involvement.', 'Diagnostic image displaying pneumothorax focused on the lung apex.', 'Clinical chest x-ray with pneumothorax showing apical air collection.']</p> <p>3. H3_basilar_components: ['Chest x-ray showing pneumothorax with basilar component.', 'Image of a lung with pneumothorax affecting the base.', 'Chest radiograph of pneumothorax with basal involvement.', 'Diagnostic image displaying pneumothorax focused on the lung base.', 'Clinical chest x-ray with pneumothorax showing basilar air collection.']</p> <p>4. H4_subcutaneous_emphysema: ['Chest x-ray showing pneumothorax with subcutaneous emphysema.', 'Image of a lung with pneumothorax and visible subcutaneous air.', 'Chest radiograph of pneumothorax associated with subcutaneous emphysema.', 'Diagnostic image displaying pneumothorax with subcutaneous air pockets.', 'Clinical chest x-ray with pneumothorax and subcutaneous emphysema evident.~']</p> <p>5. H5_size_descriptors: ['Chest x-ray showing a small pneumothorax.', 'Image of a lung with a moderate pneumothorax.', 'Chest radiograph of a large pneumothorax.', 'Diagnostic image displaying a substantial pneumothorax.', 'Clinical chest x-ray with a minimal pneumothorax.~']</p> | <p>Hypotheses:</p> <p>The classifier is making mistake as it is biased toward:</p> <p>H1: loculated characteristics of pneumothorax</p> <p>H2: presence of chest tubes</p> <p>H3: fluid levels in pneumothorax</p> <p>H4: size and extent descriptions of pneumothorax</p> <p>H5: side of the body affected by pneumothorax</p> <p>Prompt to test each hypotheses:</p> <p>1. H1_loculated_characteristics_of_pneumothorax: ['Chest X-ray showing loculated pneumothorax with varying air and fluid levels', 'Loculated air pockets in pneumothorax as seen in a chest radiograph', 'Pneumothorax with loculated air collections complicating the diagnosis', 'Loculated pneumothorax with complex air and fluid separation', 'Detailed view of loculated pneumothorax with chest tube intervention']</p> <p>2. H2_presence_of_chest_tubes: ['Chest X-ray with visible chest tubes in place for pneumothorax treatment', 'Pneumothorax management with chest tubes as seen in the radiograph', 'Chest radiograph depicting the placement of chest tubes in pneumothorax', 'Influence of chest tubes on the appearance of pneumothorax in X-ray images', 'Chest tubes in situ for a patient with pneumothorax on the radiograph']</p> <p>3. H3_fluid_levels_in_pneumothorax: ['Chest X-ray showing pneumothorax with significant fluid levels', 'Pneumothorax with varying degrees of fluid accumulation in chest X-ray', 'Radiographic appearance of pneumothorax with fluid levels', 'Assessment of fluid levels in pneumothorax via chest radiography', 'Fluid levels indicating severity of pneumothorax in a chest X-ray']</p> <p>4. H4_size_and_extent_descriptions_of_pneumothorax: ['Chest X-ray showing a large pneumothorax covering extensive lung area', 'Moderate sized pneumothorax visible on the right side in chest X-ray', 'Small apical pneumothorax detected in a routine chest X-ray', 'Extent of pneumothorax as a critical factor in chest X-ray analysis', 'Evaluating the size and spread of pneumothorax in chest radiographs']</p> <p>5. H5_side_of_the_body_affected_by_pneumothorax: ['Right-sided pneumothorax as shown in chest X-ray imaging', 'Left basal pneumothorax detected in a diagnostic chest X-ray', 'Chest X-ray revealing pneumothorax on the left side of the chest', 'Comparison of right and left side pneumothorax in X-ray images', 'Implications of pneumothorax location on the left side in chest X-rays']</p> |

Figure 11: Comparison of hypothesis generation and testing using different variants of CXR-CLIP. We highlight the common attributes for both variants in yellow.

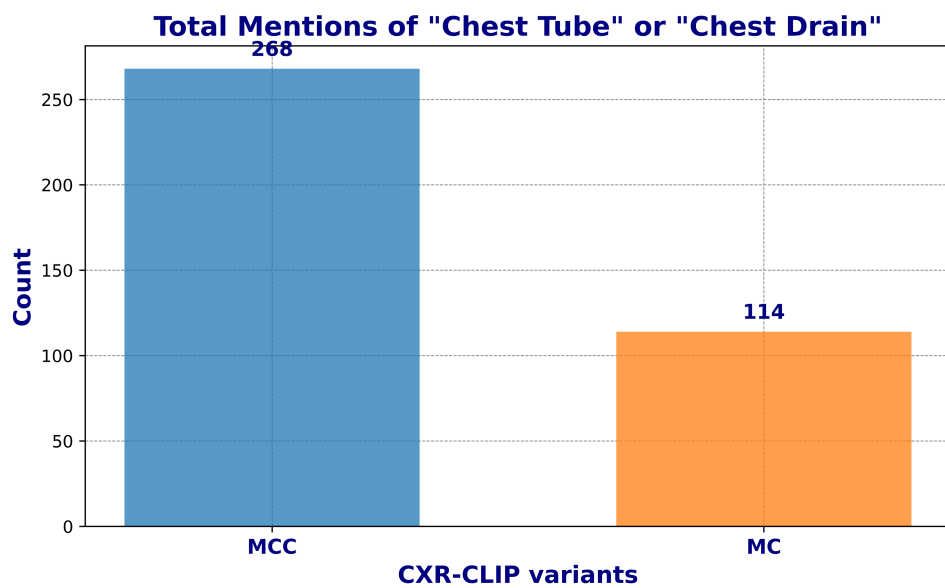


Figure 12: Comparison of “chest tube” and “chest drain” mentions in sentences retrieved using different CXR-CLIP variants. The MCC variant shows a significantly higher count, highlighting differences in dataset composition during the pretraining and its impact on the model’s bias detection.

B.9.4 Closest hypothesis to the ground truth attribute

Tables 5 and 4 show the top3 hypotheses for RN50 (convolution-based) and ViT (transformer-based) architectures, respectively. These hypotheses are the most similar to the ground truth attribute on which the source model f is biased.

Table 4: Top 3 associated hypotheses for the ground truth biased attribute for ViTs on various datasets

| Dataset (Label) | Attribute | Top 3 hypotheses |
|------------------------|-----------|---|
| Waterbirds (waterbird) | Water | 1. activities like swimming or flying
2. conditions like cloudy or sunny
3. presence of objects like boats or rocks |
| Waterbirds (landbird) | Land | 1. bird in the middle of a forest
2. yellow bird
3. bird sitting on top of a tree |
| CelebA (Blonde) | Women | 1. woman with black top
2. woman with white top
3. woman wearing a black jacket |
| MetaShift (Dog) | Outdoor | 1. presence of a leash
2. presence of a ball
3. presence of a car |
| MetaShift (Cat) | Indoor | 1. beds
2. windows
3. televisions |

Table 5: Top 3 associated hypotheses for the ground truth biased attribute for CNNs on various datasets

| Dataset (Label) | Attribute | Top 3 hypotheses |
|------------------------|---------------|---|
| Waterbirds (waterbird) | Water | 1. water bodies like oceans and lakes
2. actions like flying or sitting
3. conditions, e.g., cloudy skies |
| Waterbirds (landbird) | Land | 1. bird being in flight
2. bird perching on top of a tree
3. bird perching on a tree branch |
| CelebA (Blonde) | Women | 1. woman with long hair
2. woman with blue eyes
3. woman wearing a black jacket |
| MetaShift (Dog) | Outdoor | 1. dogs in motion
2. dogs on leashes
3. beach environments |
| MetaShift (Cat) | Indoor | 1. televisions
2. windows
3. beds |
| NIH (pneumothorax) | Chest tube | 1. the presence of chest tubes
2. loculated pneumothorax
3. size and extent of pneumothorax |
| RSNA-Mammo (cancer) | Calcification | 1. scattered calcifications
2. vascular calcifications
3. bilateral occurrences |

B.9.5 Extended qualitative results for our slice discovery method on various datasets

Figures 13, 14, 15, 16, and 17 provide qualitative illustrations of our method applied to various datasets using RN50 models. Specifically, they showcase the classification of "landbird" from the Waterbirds dataset, "blond" from CelebA, "cat" and "dog" from MetaShift, and "cancer" from the RSNA dataset, respectively. Meanwhile, Figures 19, 18, 20, and 21 present similar qualitative insights for "landbird" and "waterbird" from the Waterbirds dataset, as well as "blond" from CelebA, all through the lens of ViT-based architectures. We find consistent patterns in the generated hypotheses across different architectures of the source model f .

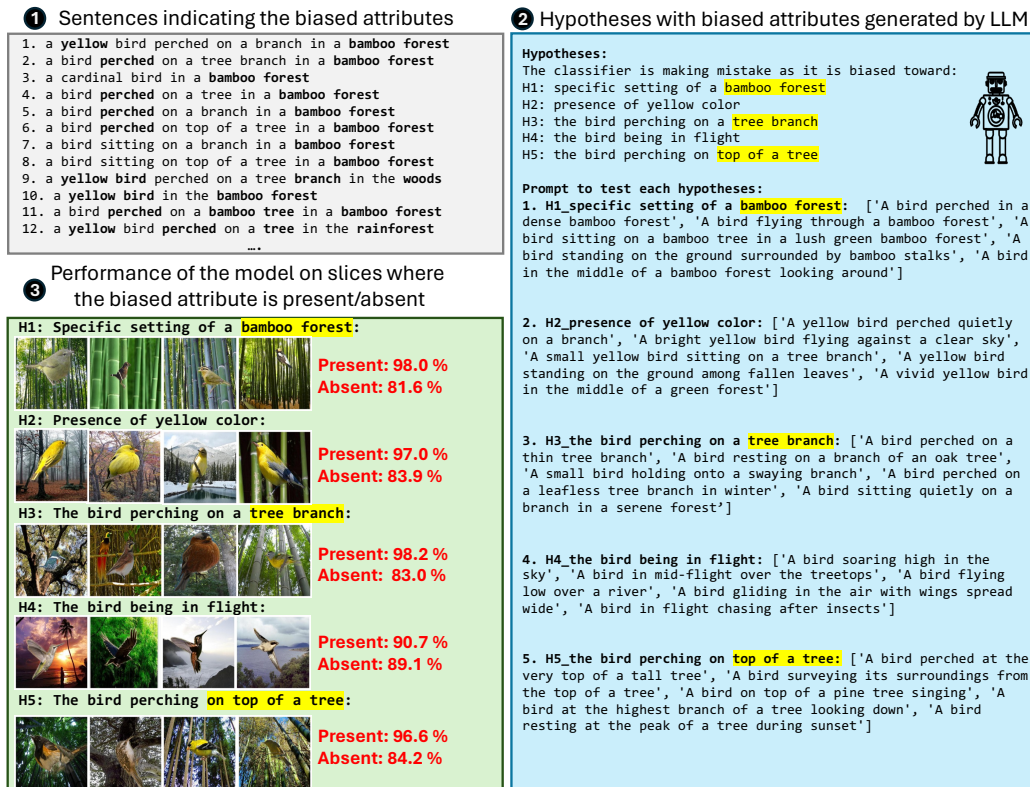


Figure 13: Slice discovery for biased attributes in RN50-based classifier for *landbird* classification in **Waterbirds** dataset. This figure details the discovery process for biased attributes involving sentence analysis, hypothesis generation by an LLM, and the model’s performance on slices where attributes are present or absent, demonstrating how biases affect classifier accuracy. We highlight the hypotheses indicative of the ground truth biased attribute (*e.g.*, land for landbirds) in **yellow**.

B.9.6 Extended results on comparing different error mitigation strategies using ViT-based models

Tab. 6 compares different error mitigation algorithms for ViT based models (f).

B.9.7 Extended results on performance improvement across various slices

Fig. 22 illustrates performance improvement across various slices of CelebA and RSNA datasets for RN50 and EN-B5 models (f) respectively. Fig. 23 illustrates the same for ViT-based models (f).

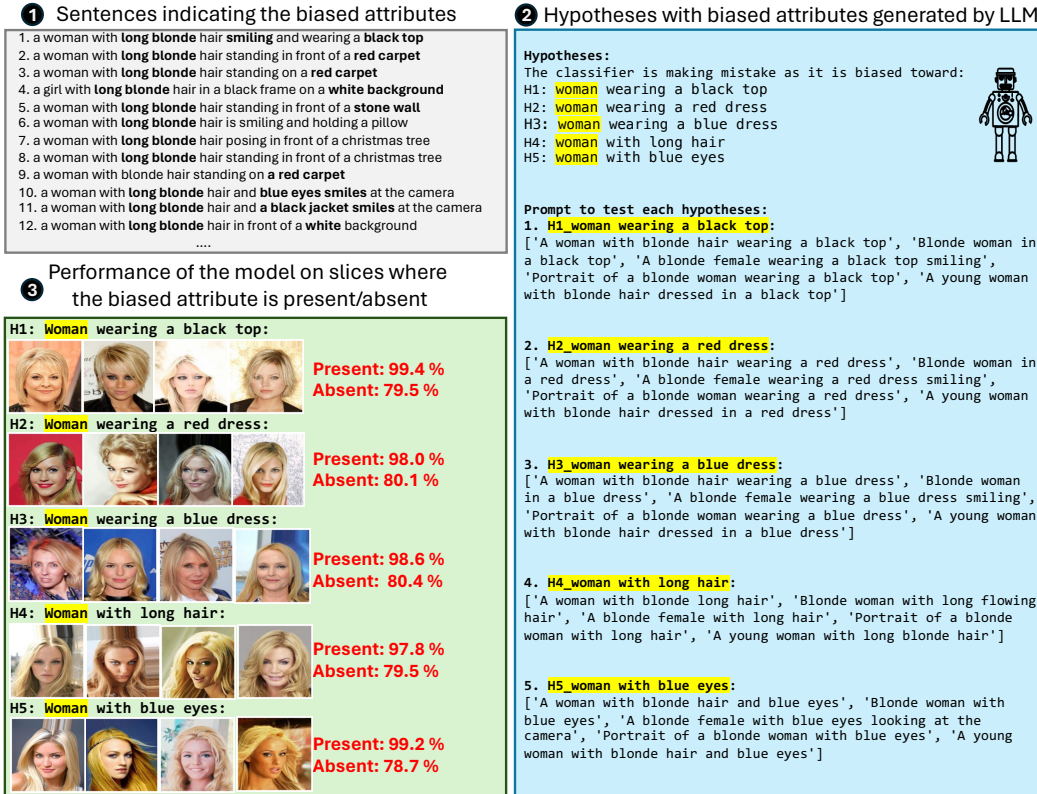


Figure 14: Slice discovery for biased attributes in RN50-based classifier for *blond* classification in **CelebA** dataset. This figure details the discovery process for biased attributes involving sentence analysis, hypothesis generation by an LLM, and the model’s performance on slices where attributes are present or absent, demonstrating how biases affect classifier accuracy. We highlight the hypotheses indicative of the ground truth biased attribute (e.g., woman for blond) in **yellow**.

Table 6: Performance comparison of ViT-based error mitigation methods, measured over 3 seeds. We highlight the best results in bold and the second best in underlined.

| Method | Waterbirds | | CelebA | |
|--------------------------|-------------|-------------|-------------|-------------|
| | Mean(%) | WGA(%) | Mean(%) | WGA(%) |
| Vanilla (ERM) | 82.7 | 51.2 | 95.2 | 46.8 |
| Mixup | 81.8 | 44.9 | 95.8 | 48.3 |
| IRM | 79.8 | 54.5 | 85.1 | 48.7 |
| MMD | 83.6 | 42.5 | 95.6 | 54.2 |
| JTT | 81.7 | 49.1 | 94.8 | 52.7 |
| GroupDRO | 82.2 | 53.1 | 93.5 | 80.1 |
| CVaRDRO | 83.5 | 46.6 | 95.6 | 55.1 |
| LISA | 83.7 | 48.8 | 95.6 | 60.2 |
| DFR _{val} | 85.0 | 76.2 | 91.3 | 81.1 |
| DFR w/ slice info (ours) | 85.1 | 81.4 | 89.1 | 79.8 |
| DFR w/ seq tune (ours) | 85.3 | 86.5 | 87.3 | 79.4 |
| DFR w/ ensemble (ours) | 84.6 | 83.3 | 88.5 | 78.6 |

1 Sentences indicating the biased attributes

1. a cat **sleeping** on top of a **computer mouse**
2. a cat **sleeping** on a **desk** in an **office**
3. a cat **sleeping** on top of a **laptop computer**
4. a cat **laying** on top of a **computer keyboard**
5. a cat **laying** on top of a **computer** on a **desk**
6. a cat **laying** on top of a **laptop computer**
7. a cat **sleeping** on top of a **laptop**
8. a cat **laying** in a **bathroom sink**
9. a cat **laying** on a **laptop computer**
10. a cat **laying** on top of a laptop on a **bed**
11. a cat **sitting** in a sink in a **bathroom**
12. a cat **laying** on a bed next to a **book**

2 Hypotheses with biased attributes generated by LLM

Hypotheses:
 The classifier is making mistake as it is biased toward:

H1: **laptops**
 H2: **bathroom settings**
 H3: **beds**
 H4: **desks**
 H5: **sinks**
 H6: sitting positions



Prompt to test each hypotheses:

1. **H1_laptops:** ['a cat sitting on a laptop in a bright room', 'a cat lying on a laptop on a desk', 'a cat sleeping next to a laptop on a couch', 'a cat playing with a laptop in a home setting', 'a cat watching the screen of a laptop']
2. **H2_bathroom settings:** ['a cat sitting on a bathroom counter', 'a cat playing with a shower curtain', 'a cat sleeping on a bathroom rug', 'a cat exploring a bathroom shelf', 'a cat inside a bathtub']
3. **H3_beds:** ['a cat lying on a bed with pillows', 'a cat playing on a bed next to a window', 'a cat sleeping on a large bed in a bedroom', 'a cat sitting on a bed next to a book', 'a cat under the blanket on a bed']
4. **H4_desks:** ['a cat sitting on a wooden desk', 'a cat lying under a desk lamp', 'a cat playing with papers on a desk', 'a cat napping on a cluttered desk', 'a cat watching a mouse on a desk']
5. **H5_sinks:** ['a cat sitting in a bathroom sink', 'a cat drinking water from a kitchen sink', 'a cat playing in a sink with a dripping faucet', 'a cat lying in a sink in a tiled bathroom', 'a cat hiding in a sink']
6. **H6_sitting positions:** ['a cat sitting upright on a couch', 'a cat sitting on a window sill', 'a cat sitting in a box', 'a cat sitting on a pillow', 'a cat sitting in a sunlit spot']

3 Performance of the model on slices where the biased attribute is present/absent

H1: Laptops:



Present: 99.4 %
Absent: 83.5 %

H2: Bathroom settings:



Present: 99.0 %
Absent: 83.1 %

H3: Beds:



Present: 98.3 %
Absent: 84.4 %

H4: Desks:



Present: 99.4 %
Absent: 82.5 %

H5: Sinks:



Present: 99.0 %
Absent: 81.7 %

Figure 15: Slice discovery for biased attributes in RN50-based classifier for classifying *cat* in **MetaShift** dataset. This figure details the discovery process for biased attributes involving sentence analysis, hypothesis generation by an LLM, and the model’s performance on slices where attributes are present or absent, demonstrating how biases affect classifier accuracy. We highlight the hypotheses indicative of the ground truth biased attribute (*e.g.*, indoor for cat) in **yellow**.

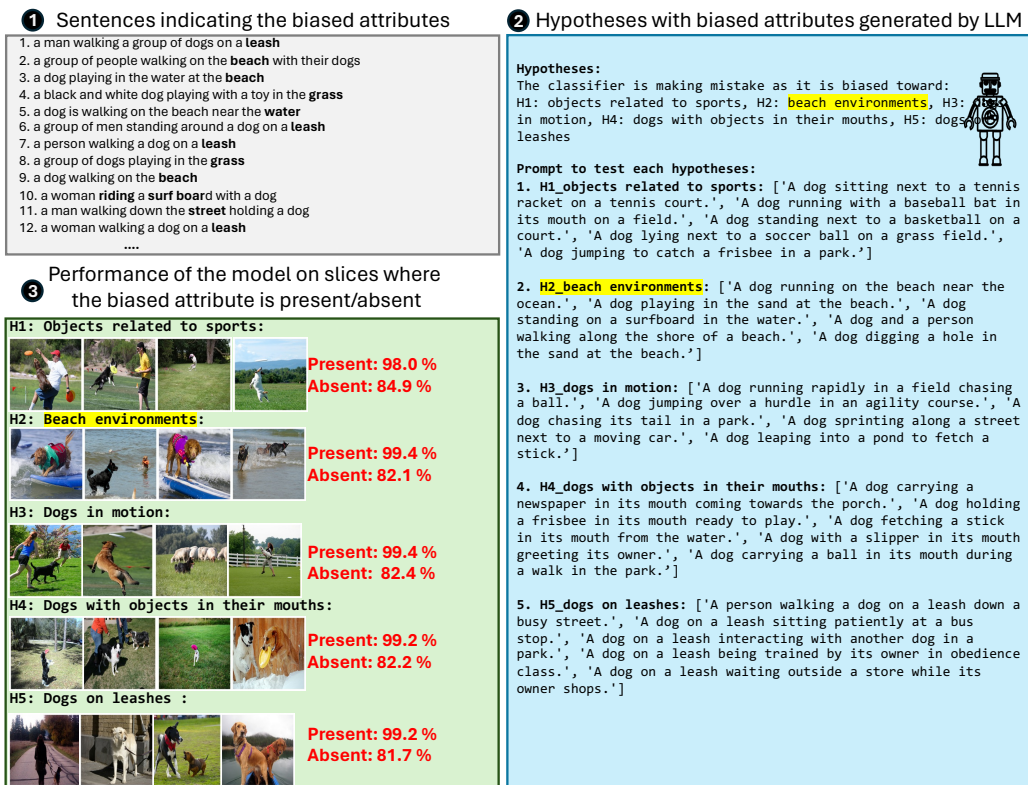


Figure 16: Slice discovery for biased attributes in RN50-based classifier for *dog* classification in **MetaShift** dataset. This figure details the discovery process for biased attributes involving sentence analysis, hypothesis generation by an LLM, and the model’s performance on slices where attributes are present or absent, demonstrating how biases affect classifier accuracy. We highlight the hypotheses indicative of the ground truth biased attribute (e.g., outdoor for dog) in **yellow**.

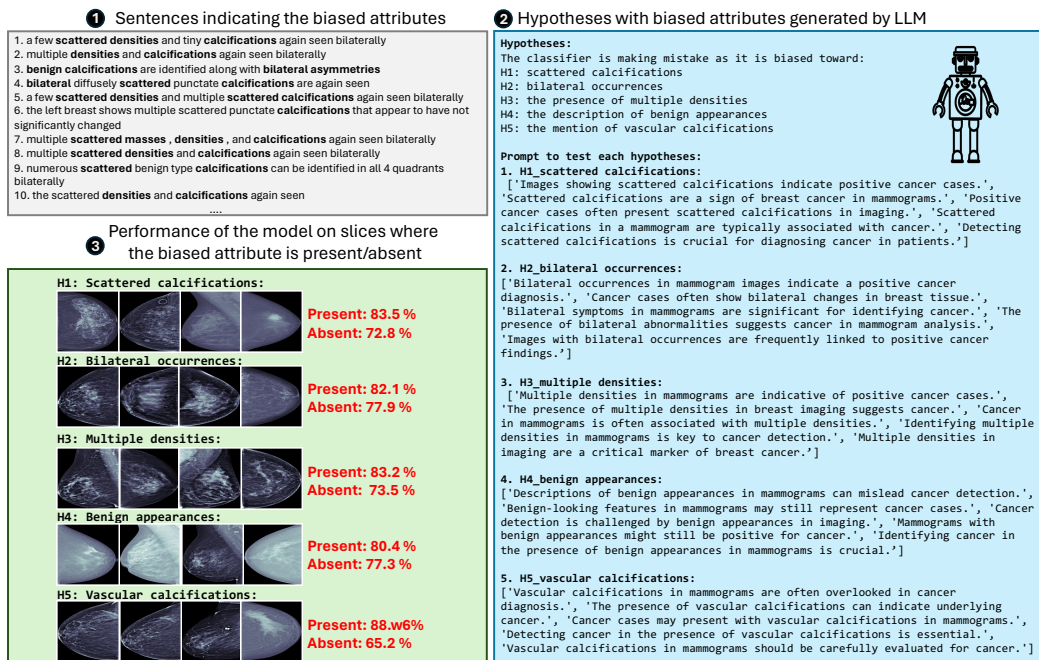


Figure 17: Slice discovery for biased attributes in RN50-based classifier for *cancer* classification in **RSNA-Mammo** dataset. This figure details the discovery process for biased attributes involving sentence analysis, hypothesis generation by an LLM, and the model’s performance on slices where attributes are present or absent, demonstrating how biases affect classifier accuracy. We highlight the hypotheses indicative of the ground truth biased attribute (e.g., calcification for cancer) in yellow.

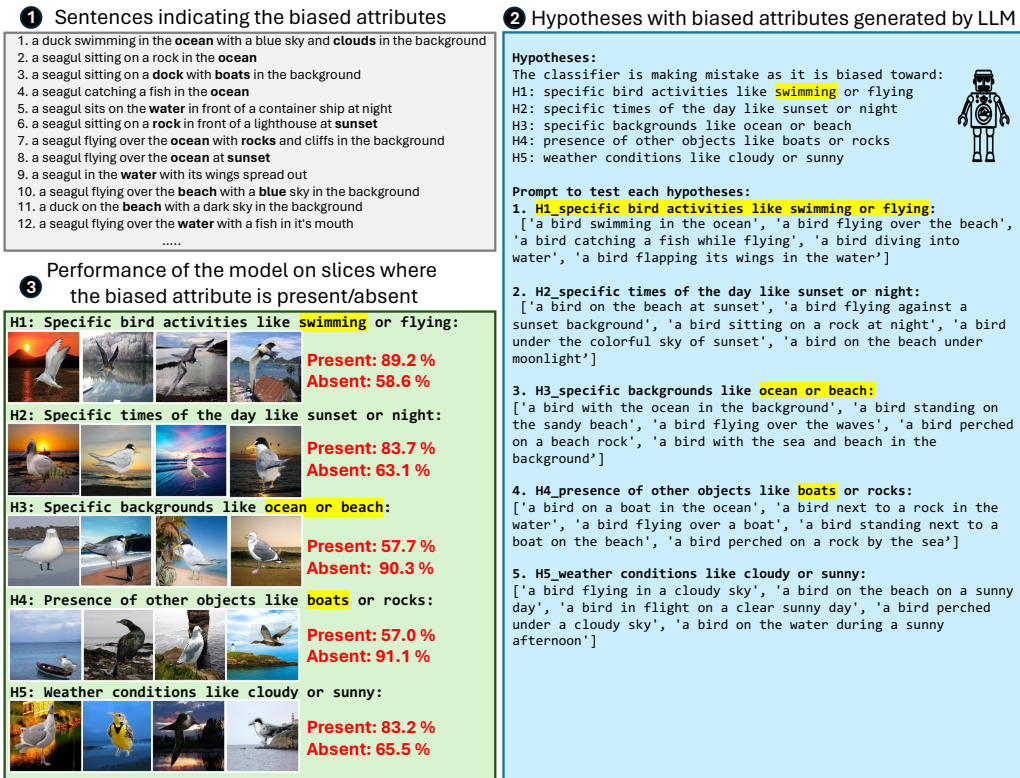


Figure 18: Slice discovery for biased attributes in ViT-based classifier for *waterbird* classification in **Waterbirds** dataset. This figure details the discovery process for biased attributes involving sentence analysis, hypothesis generation by an LLM, and the performance of the model on slices where attributes are present or absent, demonstrating how biases affect classifier accuracy. We highlight the hypotheses indicative of the ground truth biased attribute (e.g., **water** for waterbirds) in **yellow**.

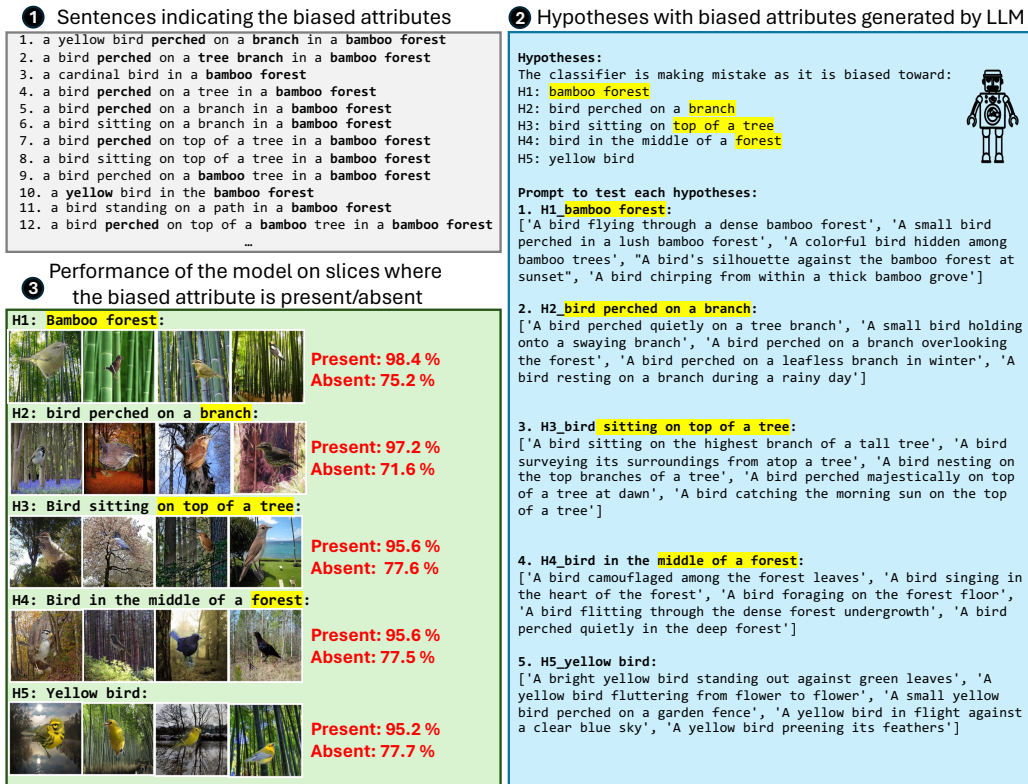


Figure 19: Slice discovery for biased attributes in ViT-based classifier for *landbird* classification in **Waterbirds** dataset. This figure details the discovery process for biased attributes involving sentence analysis, hypothesis generation by an LLM, and the model’s performance on slices where attributes are present or absent, demonstrating how biases affect classifier accuracy. We highlight the hypotheses indicative of the ground truth biased attribute (e.g., land for landbirds) in **yellow**.

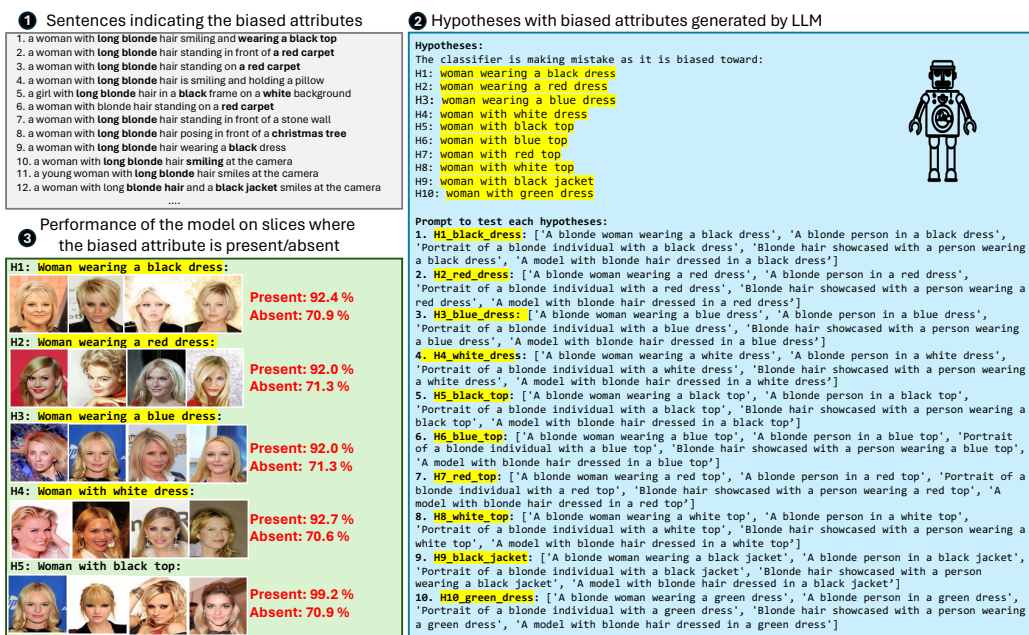


Figure 20: Slice discovery for biased attributes in ViT-based classifier for *blond* classification in **CelebA** dataset. This figure details the discovery process for biased attributes involving sentence analysis, hypothesis generation by an LLM, and the model’s performance on slices where attributes are present or absent, demonstrating how biases affect classifier accuracy. We highlight the hypotheses indicative of the ground truth biased attribute (e.g., woman for blond) in **yellow**.

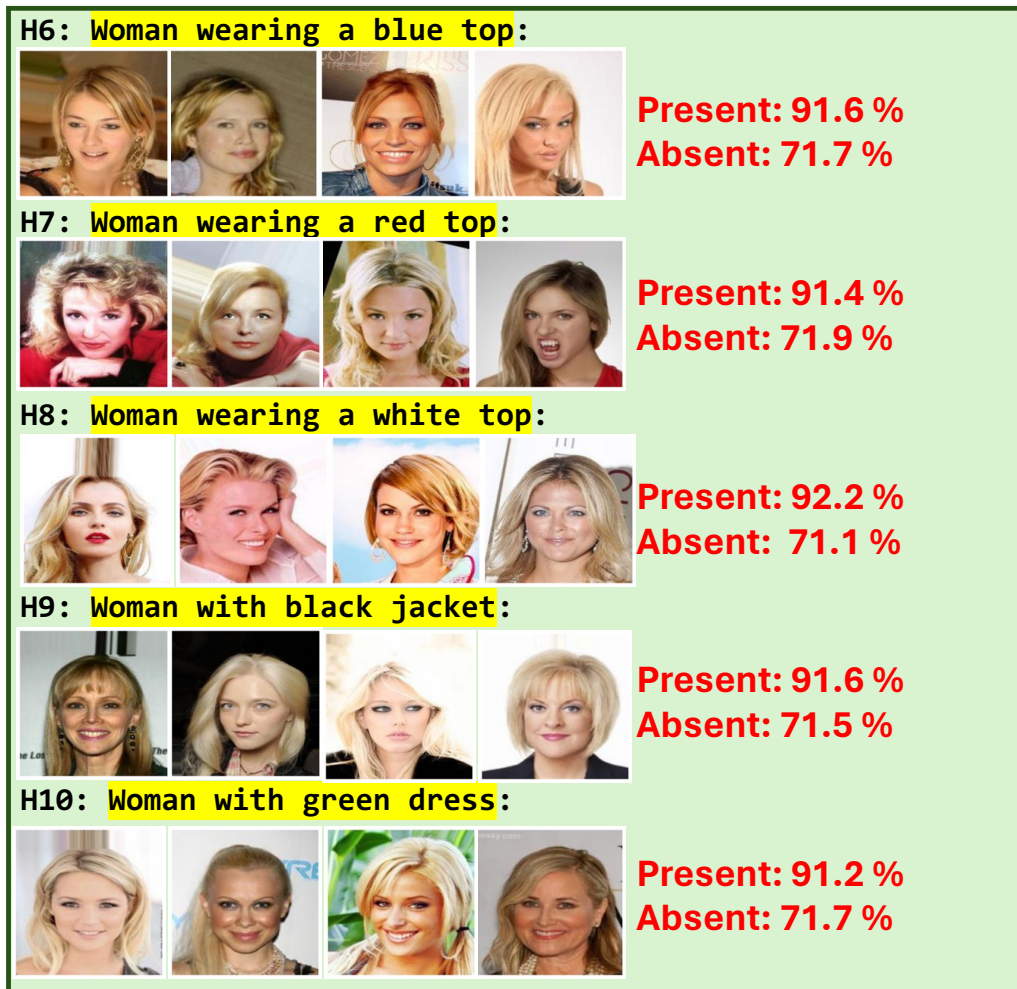


Figure 21: Performance of the ViT-based classifier on additional slices where attributes are present/absent for *blond* classification in **CelebA** dataset.

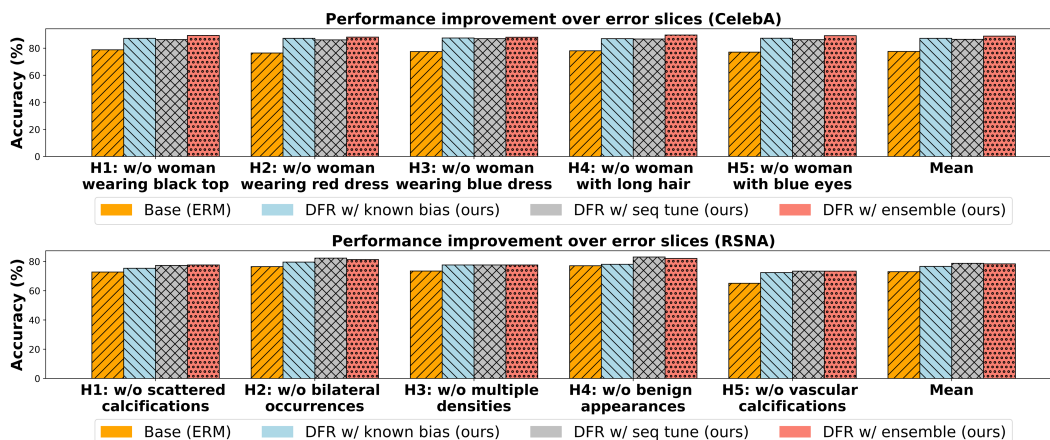


Figure 22: Accuracy improvements over error slices for our mitigation strategies compared to ERM for RN50 and EN-B5 based models (f) for the CelebA and RSNA datasets, respectively.

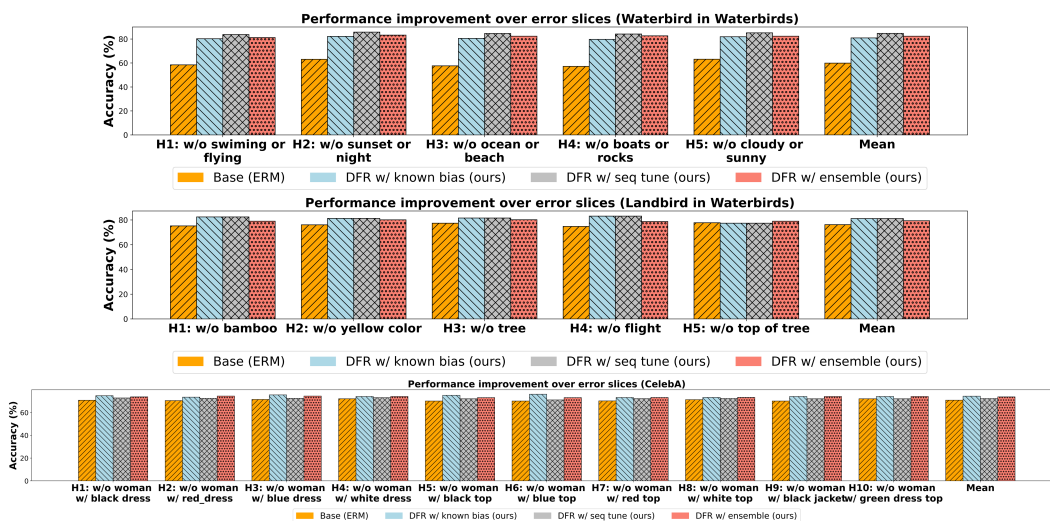


Figure 23: Accuracy improvements over error slices for our mitigation strategies compared to ERM for ViT-based models (f) for the *waterbird-landbird* and *blond* classification for Waterbirds and CelebA datasets, respectively